A simple topography-driven and calibration-free runoff generation module

3   Hongkai Gao[1,2,3,4] *, Christian Birkel [5,6], Markus Hrachowitz [7], Doerthe Tetzlaff [6], Chris Soulsby [6], Hubert H. G. Savenije[7]

5   [1] Key Laboratory of Geographic Information Science (Ministry of Education of China), East China Normal University,
6   Shanghai, China.

7   [2] School of Geographical Sciences, East China Normal University, Shanghai, China.

8   [3] Julie Ann Wrigley Global Institute of Sustainability, Arizona State University PO Box 875402. Tempe, AZ 85287-5402.

9   [4] Northwest Institute of Eco-Environment and Resources, Chinese Academy of Sciences, Lanzhou, China.

10   [5] Department of Geography, University of Costa Rica, San José, Costa Rica

11   [6] Northern Rivers Institute, University of Aberdeen, Scotland.

12   [7] Water Resources Section, Delft University of Technology, Delft, Netherlands.

14   *Corresponding to Hongkai Gao (hkgao@geo.ecnu.edu.cn)

Abstract

17   Reading landscapes and developing calibration-free runoff generation models that adequately reflect land
18   surface heterogeneities remains the focus of much hydrological research. In this study, we report a novel
19   and simple topography-driven runoff generation parameterization – the HAND-based Storage Capacity
20   curve (HSC), that uses a topographic index (HAND, Height Above the Nearest Drainage) to identify
21   hydrological similarity and the extent of saturated areas in catchments. The HSC can be used as a module
22   in any conceptual rainfall-runoff model. Further, coupling the HSC parameterization with the Mass Curve
23   Technique (MCT) to estimate root zone storage capacity (S_{uMax}), we developed a calibration-free runoff
24   generation module HSC-MCT. The runoff generation modules of HBV and TOPMODEL were used for
25   comparison purposes. The performance of these two modules (HSC and HSC-MCT) was first checked
26   against the data-rich Bruntland Burn (BB) catchment in Scotland, which has a long time series of field-
27   mapped saturation area extent. We found that HSC, HBV and TOPMODEL all perform well to reproduce
28   the hydrograph, but the HSC module performs better in reproducing saturated area variation, in terms of

29 correlation coefficient and spatial pattern. The HSC and HSC-MCT modules were subsequently tested for

30 323 MOPEX catchments in the US, with diverse climate, soil, vegetation and geological characteristics. In

31 comparison with HBV and TOPMODEL, the HSC performs better in both calibration and validation,

32 particularly in the catchments with gentle topography, less forest cover and arid climate. Despite having

33 no calibrated parameters, the HSC-MCT module performed comparably well with calibrated modules,

34 highlighting the robustness of the HSC parameterization to describe the spatial distribution of the root

35 zone storage capacity and the efficiency of the MCT method to estimate S_{uMax}. This novel and calibration-

36 free runoff generation module helps to improve the Prediction in Ungauged Basins and has great potential

37 to be generalized at the global scale.

1   Introduction

40 Determining the volume and timing of runoff generation from rainfall inputs remains a central challenge

41 in rainfall-runoff modelling (Beven, 2012; McDonnell, 2013). Creating a simple, calibration-free, but robust

42 runoff generation module has been, and continues to be, an essential pursuit of hydrological modellers.

43 Although we have made tremendous advances to enhance our ability on Prediction in Ungauged Basins

44 (PUB) (Sivapalan et al., 2003; Blöschl et al., 2013; Hrachowitz et al., 2013), it is not uncommon that models

45 become increasingly complicated in order to capture the details of hydrological processes shown by

46 empirical studies (McDonnell, 2007; Sivapalan, 2009; Yu et al., 2014). More detailed process

47 conceptualization normally demands higher data requirements than our standard climatological and

48 hydrological networks can provide, leading to more calibrated parameters and a probable increase in

49 model uncertainty (Sivapalan, 2009).

50 Hydrological connectivity is a key characteristic of catchment functioning, controlling runoff generation.

51 It is a property emerging at larger scales, describing the temporal dynamics of how spatially

52 heterogeneous storage thresholds in different parts of catchments are exceeded to contribute to storm

53 runoff generation and how they are thus "connected to the stream" (e.g. Zehe and Blöschl, 2004;

54 Bracken and Croke, 2007; Lehmann et al., 2007; Zehe and Sivapalan, 2009; Ali et al., 2013; Blume and

55 van Meerveld, 2015). Connectivity is controlled by a multitude of factors (Ali and Roy, 2010), including

56 but not limited to surface (e.g. Jencso et al., 2009) and subsurface topography (e.g. Tromp-van Meerveld

57 and McDonnell, 2006), soils (including preferential flow networks; e.g. Zehe et al., 2006; Weiler and

58 McDonnell, 2007), land cover (e.g. Imeson and Prinsen, 2004; Jencso and McGlynn, 2011; Emanuel et al.,

59   2014), the wetness state of the system (e.g. Detty and McGuire, 2010; Penna et al., 2011; McMillan et

60   al., 2014; Nippgen et al., 2015).

61   In detailed distributed hydrological bottom-up models, connectivity emerges from the interplay of

62   topography, soil type and water table depth. For example, TOPMODEL (Beven and Kirkby, 1979; Beven

63   and Freer, 2001) uses topographic wetness index (TWI) to distinguish hydrologic similarity; and SHE

64   (Abbott et al. 1986) and tRIBS (Ivanov et al. 2004; Vivoni et al. 2005) use partial differential equations to

65   describe the water movement based on pressure gradients obtained by topography; and the

66   Representative Elementary Watershed (REW) approach divides catchment into a number of REWs to

67   build balance and constitutive equations for hydrological simulation (Reggiani et al., 1999; Zhang and

68   Savenije, 2005; Tian et al., 2008). As the relevant model parameters such as local topographic slope and

69   hydraulic conductivity can, in spite of several unresolved issues for example relating to the differences in

70   the observation and modelling scales (e.g. Beven, 1989; Zehe et al., 2014), be obtained from direct

71   observations, they could *in principle* be applied without calibration.

72   Zooming out to the macro-scale, top-down models, in contrast, are based on emergent functional

73   relationships that integrate system-internal heterogeneity (Sivapalan, 2005). These functional

74   relationships require parameters that are effective on the modelling scale and that can largely not be

75   directly determined with small-scale field observations (cf. Beven, 1995), thus traditionally determined

76   by calibration. However, frequently the number of observed variables for model calibration is, if

77   available at all, limited to time series of stream flow. The absence of more variables to constrain models

78   results in such models being ill-posed inverse problems. Equifinality in parameterization and in the

79   choice of parameters then results in considerable model uncertainty (e.g. Beven, 1993, 2006). To limit

80   this problem and to also allow predictions in the vast majority of ungauged catchments, it is therefore

81   desirable to find ways to directly infer effective model parameters at the modelling scale from readily

82   available data (Hrachowitz et al., 2013).

83   The component that is central for establishing connectivity in most top-down models is the soil moisture

84   routine. Briefly, it controls the dynamics of water storage and release in the unsaturated root zone and

85   partitions water into evaporative fluxes, groundwater recharge and fast lateral storm flow generating

86   runoff (Gao et al., 2018a; Shao et al., 2018). The latter of which is critical from the aspect of connectivity.

87   In majority regions, Hortonian overland flow (HOF, i.e. infiltration excess overland flow) is of minor

88   importance(Dunne and Black, 1970; Sklash and Farvolden, 1979; Beven, 2004; Burt and McDonnell,

89   2015), even in arid regions where often most locally generated HOF is re-infiltrated while flowing on

90 hillslopes (Liu et al., 2012) and never reaches the stream channel network. Thus the term saturation

91 excess flow (SEF) can represent, depending on the model and the area of application, different

92 processes, such as saturation overland flow, preferential flow, flow through shallow, high permeability

93 soil layers or combinations thereof. The interplay between water volumes that are stored and those that

94 are released laterally to the stream via fast, connected flow paths ("connectivity") is in most top-down

95 models described by functions between water stored in the unsaturated root zone ("soil moisture") and

96 the areal proportion of heterogeneous, local storage thresholds that are exceeded and thus

97 "connected" (Zhao et al., 1980). In other words, in those parts of a catchment where the storage

98 threshold is exceeded will generate lateral flows, and can alternatively be interpreted as runoff

99 coefficient (e.g. Ponce and Hawkins, 1996; Perrin and Andreassian, 2001; Fenicia et al., 2007; Bergström

100 and Lindström, 2015). Thus the idea goes back to the variable contributing area concept, assuming that

101 only partial areas of a catchment, where soils are saturated and thus storage thresholds are exceeded,

102 contribute to runoff (Hewlett, 1961; Dunne and Black, 1970; Hewlett and Troendle, 1975). Although

103 originally developed for catchments dominated by saturation overland flow, the extension of the

104 concept to subsurface connectivity, posing that surface and subsurface connectivity are "two sides of

105 the same coin" (McDonnell, 2013), proved highly valuable for models such as Xinanjiang (Zhao et al.,

106 1980), HBV (Bergström and Forsman, 1973; Bergström and Lindström, 2015), SCS-CN (Ponce and

107 Hawkins, 1996; Bartlett et al., 2016), FLEX (Fenicia et al., 2008) and GR4J (Perrin and Andreassian et al.,

108 2001).

109 Among these models, connectivity is formulated in a general form as C_R=f($S_U(t)$,S_{uMax},β), where C_R is the

110 runoff coefficient, i.e. the proportion of the catchment generating runoff, $S_U(t)$ is the catchment water

111 content in the unsaturated root zone at any time t, S_{uMax} is a parameter representing the total storage

112 capacity in the unsaturated root zone and β is a shape parameter, representing the spatial distribution

113 of heterogeneous storage capacities in the unsaturated root zone. The parameters of these functions

114 are typically calibrated. In spite of being the core component of soil moisture routines in many top-down

115 models, little effort was previously invested to find ways to determine the parameters at the catchment-

116 scale directly from available data. An important step towards understanding and quantifying

117 connectivity pattern directly based on observations was recently achieved by intensive experimental

118 work in the Tenderfoot Creek catchments in Montana, US. In their work Jencso et al. (2009) were able to

119 show that connectivity of individual hillslopes in their headwater catchments is highly related to their

120 respective upslope accumulated areas. Using this close relationship, Smith et al. (2013) successfully

121 developed a simple top-down model with very limited need for calibration, emphasizing the value of

122 "enforcing field-based limits on model parameters" (Smith et al., 2016). Based on hydrological landscape

123 analysis, FLEX-Topo model (Savenije, 2010) can dramatically reduce the need for calibration (Gharari et

124 al., 2014), and hold considerable potential for spatial model transferability without the need for

125 parameter re-calibration (Gao et al., 2014a; H. Gao et al., 2016). In a recent development, several

126 studies suggest that S_{uMax} can be robustly and directly inferred from long term water balance data, by

127 the Mass Curve Technique (MCT) (Gao et al., 2014; de Boer-Euser et al., 2016; Nijzink et al., 2016). The

128 MCT is an engineering method for reservoir design, in which the reservoir size is estimated as a function

129 of accumulated inflow and human water demand. The MCT treats the root zone as a reservoir, and

130 estimates catchment-scale S_{uMax} from measurable hydrometeorological data, without the need for

131 further calibration. This leaves shape parameter β as the only free calibration parameter for soil

132 moisture routines of that form. Topography is often the dominant driver of water movement caused by

133 prevailing hydraulic gradients. More crucially, topography usually provides an integrating indicator for

134 hydrological behavior, since topography is usually closely related with other landscape elements, such as

135 soil vegetation climate and even geology (Seibert et al., 2007; Savenije, 2010; Rempe and Dietrich, 2014;

136 Gao et al., 2014b; Maxwell and Condon, 2016; Gomes, 2016). The Height Above the Nearest Drainage

137 (HAND; Rennó et al., 2008; Nobre et al., 2011; Gharari et al., 2011), which can be computed from readily

138 available digital elevation models (DEM), could potentially provide first order estimates of groundwater

139 depth , as there is some experimental evidence that with increasing HAND, groundwater depths

140 similarly increase (e.g. Haria and Shand, 2004; Martin et al., 2004; Molenat et al., 2005, 2008; Shand et

141 al., 2005; Condon and Maxwell, 2015; Maxwell and Condon, 2016). HAND can be interpreted as a proxy

142 of the hydraulic head and is thus potentially more hydrologically informative than the topographic

143 elevation above sea level (Nobre et al., 2011). Compared with the TWI in TOPMODEL, HAND is an

144 explicit measure of a physical feature linking terrain to water related potential energy for local drainage

145 (Nobre et al., 2011). More interestingly, topographic structure emerges as a powerful force determining

146 rooting depth under a given climate or within a biome (Figure 1), revealed by a global synthesis of 2,200

147 root observations of >1000 species (Fan et al., 2017). This leads us to think from ecological perspective

148 to use the topographic information as an indicator for root zone spatial distribution without calibrating

149 the β, and coupling it with the MCT method to estimate the S_{uMax}, eventually create a calibration-free

150 runoff generation module.

151 In this study we are therefore going to test the hypotheses that: (1) HAND can be linked to the spatial

152 distribution of storage capacities and therefore can be used to develop a new runoff generation module

153 (HAND-based Storage Capacity curve, i.e. HSC); (2) the distribution of storage capacities determined by

154 HAND contains different information than the topographic wetness index; (3) the HSC together with water
155 balance-based estimates of S_{uMax} (MCT method) allow the formulation of calibration-free
156 parameterizations of soil moisture routines in top-down models directly based on observations. All these
157 hypotheses will be tested firstly in a small data-rich experimental catchment (the Bruntland Burn
158 catchment in Scotland), and then apply the model to a wide range of larger MOPEX catchments (Model
159 Parameter Estimation Experiment).

160 This paper is structured as follows. In the Methods section, we describe two of our proposed modules, i.e.
161 HSC and HSC-MCT, and two benchmark models (HBV, TOPMODEL). This section also includes the
162 description of other modules (i.e. interception, evaporation and routing) in rainfall-runoff modelling, and
163 the methods for model evaluation, calibration and validation. The Dataset section reviews the empirically-
164 based knowledge of the Bruntland Burn catchment in Scotland and the hydrometerological and
165 topographic datasets of MOPEX catchments in the US for model comparison. The Results section presents
166 the model comparison results. The Discussion section interprets the relation between rainfall-runoff
167 processes and topography, catchment heterogeneity and simple model, and the implications and
168 limitations of our proposed modules. The conclusions are briefly reviewed in the Summary and
169 Conclusions section.

170 2 Methods

171 Based on our perceptual model that saturation excess flow (SEF) is the dominant runoff generation
172 mechanism in most cases, we developed the HAND-based Storage Capacity curve (HSC) module.
173 Subsequently, estimating the parameter of root zone storage capacity (S_{uMax}) by the MCT method without
174 calibration, the HSC-MCT was developed. In order to assess the performance of our proposed modules,
175 two widely-used runoff generation modules, i.e. HBV power function and TOPMODEL module, were set
176 as benchmarks. Other modules, i.e. interception, evaporation and routing, are kept with identical
177 structure and parameterization for the four rainfall-runoff models (HBV, TOPMODEL, HSC, HSC-MCT,
178 whose names are from their runoff generation modules), to independently diagnose the difference among
179 runoff generation modules (Clark et al., 2008; 2010).

180 2.1 Two benchmark modules

181 **HBV power function**

182 The HBV runoff generation module applies an empirical power function to estimate the nonlinear
183 relationship between the runoff coefficient and soil moisture (Bergström and Forsman, 1973; Bergström
184 and Lindström, 2015). The function is written as:

$$A_s = (\frac{S_u}{S_{uMax}})^{\beta} \tag{1}$$

186 Where A_s (-) represents the contributing area, which equals to the runoff coefficient of a certain rainfall
187 event; S_u (mm) represents the averaged root zone soil moisture; S_{uMax} (mm) is the averaged root zone
188 storage capacity of the studied catchment; β (-) is the parameter determining the shape of the power
189 function. The prior range of β can be from 0.1 to 5. The S_u - A_s has a linear relation while β equals to 1. And
190 the shape becomes convex while the β is less than 1, and the shape turns to concave while the β is larger
191 than 1. In most situations, S_{uMax} and β are two free parameters, cannot be directly measured at the
192 catchment scale, and need to be calibrated based on observed rainfall-runoff data.

193 **TOPMODEL module**

194 The TOPMODEL assumes topographic information captures the runoff generation heterogeneity at
195 catchment scale, and the TWI is used as an index to identify rainfall-runoff similarity (Beven and Kirkby,
196 1979; Sivapalan et al., 1997). Areas with similar TWI values are regarded as possessing equal runoff
197 generation potential. More specifically, the areas with larger TWI values tend to be saturated first and
198 contribute to SEF; but the areas with lower TWI values need more water to reach saturation and generate
199 runoff. The equations are written as follow:

$$D_i = \overline{D} + S_{uMax}(\overline{I_{TW}} - I_{TW_i}) \tag{2}$$

$$\overline{D} = S_{uMax} - S_u \tag{3}$$

$$A_s = \sum A_{s\_i}; \quad \text{while } D_i < 0 \tag{4}$$

203 Where D_i (mm) is the local storage deficit below saturation at specific location (i); $\overline{D}$ (mm) is the averaged
204 water deficit of the entire catchment (Equation 2), which equals to (S_{uMax} - S_u), as shown in Equation 3. I_{TWi}
205 is the local I_{TW} value. $\overline{I_{TW}}$ is the averaged TWI of the entire catchment. Equation 2 means in a certain soil
206 moisture deficit condition for the entire catchment ($\overline{D}$), the soil moisture deficit of a specific location (D_i),
207 is determined by the catchment topography (I_{TW} and I_{TWi}), and the root zone storage capacity (S_{uMax}).

208   Therefore, the areas with D_i less than zero are the saturated areas (A_{s_i}), equal to the contributing areas.

209   The integration of the A_{s_i} areas (A_s), as presented in Equation 4, is the runoff contributing area, which

210   equals to the runoff coefficient of that rainfall event.

211   Besides continuous rainfall-runoff calculation, Equations 2-4 also allow us to obtain the contributing area

212   (A_s) from the estimated relative soil moisture (S_u/S_{uMax}), and then map it back to the original TWI map,

213   which makes it possible to test the simulated contributing area by field measurement. It is worth

214   mentioning that the TOPMODEL in this study is a simplified version, and not identical to the original one,

215   which combines the saturated and unsaturated soil components.

216   2.2   HSC module

217   In the HSC module, we assume 1) primarily saturation excess flow as the dominant runoff generation

218   mechanism; 2) the local root zone storage capacity has a positive and linear relationship with HAND, from

219   which we can derive the spatial distribution of the root zone storage capacity; 3) rainfall firstly feeds local

220   soil moisture deficit, and no runoff can be generated before local soil moisture being saturated.

221   Figure 2 shows the perceptual HSC module, in which we simplified the complicated 3-D topography of a

222   real catchment into a 2-D simplified hillslope. And then derive the distribution of root zone storage

223   capacity, based on topographic analysis and the second assumption as mentioned in the preceding

224   paragraph. Figure 3 shows the approach to derive the S_u-A_s relation, which are detailed as follows.

225   I.   **Generate HAND map.** The HAND map, which represents the relative vertical distance to the

226   nearest river channel, can be generated from DEM (Gharari et al., 2011). The stream initiation

227   threshold area is a crucial parameter, determining the perennial river channel network

228   (Montgomery and Dietrich, 1989; Hooshyar et al., 2016), and significantly impacting the HAND

229   values. In this study, the start area was chosen as 40ha for the BB catchment to maintain a close

230   correspondence with observed stream network. And for the MOPEX catchments, the stream

231   initiation area threshold is set as 500 grid cells (4.05 km^2), which fills in the range of stream

232   initiation thresholds reported by others (e.g. Colombo et al., 2007; Moussa, 2008, 2009). HAND

233   maps were then calculated from the elevation of each raster cell above nearest grid cell flagged

234   as stream cell following the flow direction (Gharari et al., 2011).

235   II.   **Generate normalized HAND distribution curve.** Firstly, sort the HAND values of grid cells in

236   ascending order. Secondly, the sorted HAND values were evenly divided into n bands (e.g. 20

237   bands in this study), to make sure each HAND band has similar area. The averaged HAND value of

238   each band is regarded as the HAND value of that band. Thirdly, normalize the HAND bands, and
239   then plot the normalized HAND distribution curve (Figure 2b).

240   III.   **Distribute S_{uMax} to each HAND band (S_{uMax_i}).** As assumed, the normalized storage capacity of each
241   HAND band (S_{uMax_i}) increases with HAND value (Figure 2c). Based on this assumption, the
242   unsaturated root zone storage capacity (S_{uMax}) can be distributed to each HAND band as S_{uMax_i}
243   (Figure 3a). It is worth noting that S_{uMax} needs to be calibrated in the HSC module, but free of
244   calibration in the HSC-MCT module.

245   IV.   **Derive the S_u - A_s curve.** With the number of s saturated HAND bands (Figure 3a-c), the soil
246   moisture (S_u) can be obtained by Equation 5; and saturated area proportion (A_s) can be obtained
247   by Equation 6.

$$S_u = \frac{1}{n}[\sum_{i=1}^{s} S_{uMax\_i} + S_{uMax\_s}(n-s)] \tag{5}$$

$$A_s = \frac{s}{n} \tag{6}$$

250   Where S_{uMax_s} is the maximum S_{uMax_i} of all the saturated HAND bands. Subsequently, the A_s - S_u
251   curve can be derived, and shown in Figure 3d.

252 The SEF mechanism assumes that runoff is only generated from saturation areas, therefore the proportion
253 of saturation area is equal to the runoff coefficient of that rainfall-runoff event. Based on the S_u-A_s curve
254 in Figure 3d, generated runoff can be calculated from root zone moisture (S_u). The HSC module also allows
255 us to map out the fluctuation of saturated areas by the simulated catchment average soil moisture. For
256 each time step, the module can generate the simulated root zone moisture for the entire basin (S_u). Based
257 on the S_u-A_s relationship (Figure 3d), we can map S_u back to the saturated area proportion (A_s) and then
258 visualize it in the original HAND map. Based on this conceptual model, we developed the computer
259 program and created a procedural module. The technical roadmap can be found in Figure 4.

260 ## 2.3   HSC-MCT module
261 The S_{uMax} is an essential parameter in various hydrological models (e.g. HBV, Xinanjiang, GR4J), which
262 determines the long-term partitioning of rainfall into infiltration and runoff. Gao et al., 2014a found that
263 S_{uMax} represents the adaption of ecosystems to local climate. Ecosystems may design their S_{uMax} based on
264 the precipitation pattern and their water demand. The storage is neither too small to be mortal in dry
265 seasons, nor too large to consume excessive energy and nutrients. Based on this assumption, we can
266 estimate the S_{uMax} without calibration, by the MCT method, from climatological and vegetation
267 information. More specifically, the average annual plant water demand in the dry season (S_R) is

268   determined by the water balance and the vegetation phenology, i.e. precipitation, runoff and seasonal

269   NDVI. Subsequently, based on the annual S_R, the Gumbel distribution (Gumbel, 1935), frequently used for

270   estimating hydrological extremes, was used to standardize the frequency of drought occurrence. S_{R20y}, i.e.

271   the root zone storage capacity required to overcome a drought once in 20 years, is used as the proxy for

272   S_{uMax} due to the assumption of a "cost" minimization strategy of plants as we mentioned above (Milly,

273   1994), and the fact that S_{R20y} has the best fit with S_{uMax} . The S_{R20y} of the MOPEX catchments can be found

274   in the map of (Gao et al., 2014a).

275   Eventually, with the MCT approach to estimate S_{uMax} and the HSC curve to represent the root zone storage

276   capacity spatial distribution, the HSC-MCT runoff generation module is created, without free parameters.

277   It is worth noting that both the HSC-MCT and HSC modules are based on the HAND derived S_u-A_s relation,

278   and their distinction lays in the methods to obtain S_{uMax}. So far, the HBV power function module has 2 free

279   parameters (S_{uMax}, β). While the TOPMODEL and the HSC both have one free parameter (S_{uMax}). Ultimately

280   the HSC-MCT has no free parameter.

281   2.4   Interception, evaporation and routing modules

282   Except for the runoff generation module in the root zone reservoir (S_{UR}), we need to consider other

283   processes, including interception (S_{IR}) before the S_{UR} module, evaporation from the S_{UR} and the response

284   routine (S_{FR} and S_{SR}) after runoff generation from S_{UR} (Figure 5). Precipitation is firstly intercepted by

285   vegetation canopies. In this study, the interception was estimated by a threshold parameter (S_{iMax}), set to

286   2 mm (Gao et al., 2014a), below which all precipitation will be intercepted and evaporated (Equation 9)

287   (de Groen and Savenije, 2006). For the S_{UR} reservoir, we can either use the HBV beta-function (Equation

288   12), the runoff generation module of TOPMODEL (Equation 2-4) or the HSC module (Section 2.3) to

289   partition precipitation into generated runoff (R_u) and infiltration. The actual evaporation (E_a) from the soil

290   equals to the potential evaporation (E_p), if S_u/S_{uMax} is above a threshold (C_e), where S_u is the soil moisture

291   and S_{uMax} is the catchment averaged storage capacity. And E_a linearly reduces with S_u/S_{uMax}, while S_u/S_{uMax}

292   is below C_e (Equation 13). The E_p can be calculated by the Hargreaves equation (Hargreaves and Samani,

293   1985), with maximum and minimum daily temperature as input. The generated runoff (R_u) is further split

294   into two fluxes, including the flux to the fast response reservoir (R_f) and the flux to the slow response

295   reservoir (R_s), by a splitter (D) (Equation 14, 15). The delayed time from rainfall peak to the flood peak is

296   estimated by a convolution delay function, with a delay time of T_{lagF}. Subsequently, the fluxes into two

297   different response reservoirs (S_{FR} and S_{SR}) were released by two linear equations between discharge and

298   storage (Equation 19, 21), representing the fast response flow and the slow response flow mainly from

299 groundwater reservoir. The two discharges (Q_f and Q_s) generated the simulated streamflow (Q_m). The

300 model parameters are shown in Table 1, while the equations are given in Table 2. More detailed

301 description of the model structure can be referred to Gao et al., 2014b and 2016. It is worth underlining

302 that the only difference among the benchmark HBV type, TOPMODEL type, HSC, and HSC-MCT models is

303 their runoff generation modules. Eventually, there are 7 free parameters in HBV model, 6 in TOPMODEL

304 and HSC model, and 5 in the HSC-MCT model.

2.5 Model evaluation, calibration, validation and models comparison

306 Two objective functions were used to evaluate model performance, since multi-objective evaluation is a

307 more robust approach to quantifying model performance with different criteria than a single one. The

308 Kling-Gupta efficiency (Gupta *et al.*, 2009) (I_{KGE}) was used as the criteria to evaluate model performance

309 and as an objective function for calibration. The equation is written as:

310
$$I_{\mathrm{KGE}} = 1 - \sqrt{(r-1)^2 + (\alpha-1)^2 + (\varepsilon-1)^2} \tag{7}$$

311 Where r is the linear correlation coefficient between simulation and observation; α ($\alpha = \sigma_{\mathrm{m}} / \sigma_{\mathrm{o}}$) is a

312 measure of relative variability in the simulated and observed values, where σ_m is the standard deviation

313 of simulated streamflow, and σ_o is the standard deviation of observed streamflow; ε is the ratio between

314 the average value of simulated and observed data. And the I_{KGL} (I_{KGE} of the logarithmic flows) (Fenicia et

315 al., 2007; Gao et al., 2014b) is used to evaluate the model performance on baseflow simulation.

316 A multi-objective parameter optimization algorithm (MOSCEM-UA) (Vrugt et al., 2003) was applied for

317 the calibration. The parameter sets on the Pareto-frontier of the multi-objective optimization were

318 assumed to be the behavioral parameter sets and can equally represent model performance. The

319 averaged hydrograph obtained by all the behavioral parameter sets were regarded as the simulated result

320 of that catchment for further studies. The number of complexes in MOSCEM-UA were set as the number

321 of parameters (7 for HBV, 6 for TOPMODEL and the HSC model, and 5 for HSC-MCT model), and the

322 number of initial samples was set to 210 and a total number of 50000 model iterations for all the

323 catchment runs. For each catchment, the first half period of data was used for calibration, and the other

324 half was used to do validation.

325 In module comparison, we defined three categories: if the difference of I_{KGE} of model A and model B in

326 validation is less than 0.1, model A and B are regarded as "equally well". If the I_{KGE} of model A is larger

327   than model B in validation by 0.1 or more, model A is regarded as outperforming model B. If the I_{KGE} of

328   model A is less than model B in validation by -0.1 or less, model B is regarded as outperforming model A.

3   Dataset

3.1   The Bruntland Burn catchment

331   The 3.2 km^2 Bruntland Burn catchment (Figure 6), located in north-eastern Scotland, was used as a

332   benchmark study to test the model's performance based on a rich data base of hydrological

333   measurements. The Bruntland Burn is a typical upland catchment in North West Europe (e.g. Birkel et al.,

334   2010), namely a combination of steep and rolling hillslopes and over-widened valley bottoms due to the

335   glacial legacy of this region. The valley bottom areas are covered by deep (in parts > 30m) glacial drift

336   deposits (e.g. till) containing a large amount of stored water superimposed on a relatively impermeable

337   granitic solid geology (Soulsby et al., 2016). Peat soils developed (> 1m deep) in these valley bottom areas,

338   which remain saturated throughout most of the year with a dominant near-surface runoff generation

339   mechanism delivering runoff quickly via micro-topographical flow pathways connected to the stream

340   network (Soulsby et al., 2015). Brown rankers, peaty rankers and peat soils are responsible for a flashy

341   hydrological regime driven by saturation excess overland flow, while humus iron podzols on the hillslopes

342   do not favor near-surface saturation but rather facilitate groundwater recharge through vertical water

343   movement (Tetzlaff et al., 2014). Land-use is dominated by heather moorland, with smaller areas of rough

344   grazing and forestry on the lower hillslopes. Its annual precipitation is 1059 mm, with the summer months

345   (May-August) generally being the driest (Ali et al., 2013). Snow makes up less than 10% of annual

346   precipitation and melts rapidly below 500m. The evapotranspiration is around 400 mm per year and

347   annual discharge around 659 mm. The daily precipitation, potential evaporation, and discharge data range

348   from January 1 in 2008 to September 30 in 2014. The calibration period is from January 1, 2008 to

349   December 31, 2010, and the data from January 1, 2011 to September 30, 2014 is used as validation.

350   The LiDAR-derived DEM map with 2m resolution shows elevation ranging from 250m to 539m (Figure 6).

351   There are 7 saturation area maps (Figure 7) (May 2, July 2, August 4, September 3, October 1, November

352   26, in 2008, and January 21, in 2009), measured directly by the "squishy boot" method and field mapping

353   by global positioning system (GPS), to delineate the boundary of saturation areas connected to the stream

354   network (Birkel et al., 2010; Ali et al., 2013). These saturation area maps revealed a dynamic behavior of

355   expanding and contracting areas connected to the stream network that were used as a benchmark test

356   for the HSC module.

3.2 MOPEX catchments

The MOPEX dataset was collected for a hydrological model parameter estimation experiment (Duan et al., 2006; Schaake et al., 2006), containing 438 catchments in the CONUS (Contiguous United States). The longest time series range from 1948 to 2003. 323 catchments were used in this study (see the name list in SI), with areas between 67 and 10,329 km^2, and excluding the catchments with data records <30 years, impacted by snowmelt or with extreme arid climate (aridity index $E_p/P > 2$). In order to analyze the impacts of catchment characteristics on model performance, excluding hydrometeorology data, we also collected the datasets of topography, depth to rock, soil texture, land use, and stream density (Table 3). These characteristics help us to understand in which catchments the HSC performs better or worse than the benchmark models.

Hydrometeorology

The dataset contains the daily precipitation, daily maximum and minimum air temperature, and daily streamflow. The daily streamflow was used to calibrate the free parameters and validate the models.

Topography

The Digital Elevation Model (DEM) of the CONUS in 90m resolution was download from the Earth Explorer of United States Geological Survey (USGS, http://earthexplorer.usgs.gov/). The HAND and TWI map can be generated from DEM. The averaged elevation and HAND are used to as two catchment characteristics.

Soil texture

In this study, soil texture is synthetically represented by the K factor, since the K factor is a lumped soil erodibility factor which represents the soil profile reaction to soil detachment (Renard et al., 2011). Generally, the soils (high in clay and sand) have low K values, and soils with high silt content have larger K values. The averaged K factor for each catchment was calculated from soil survey information available from USGS (Wolock, 1997).

Land use

Land use data was obtained from National Land Cover Database (NLCD, http://www.mrlc.gov/nlcd.php). Forest plays an essential role in hydrological processes (Gao et al., 2018a), especially for the runoff generation (Brooks et al., 2010). Forest area proportion was utilized as an integrated indictor to represent the impact of vegetation cover on hydrological processes.

385 **Stream density**

386 Stream density (km/km^2) is the total length of all the streams and rivers in a drainage basin divided by the
387 total area of the drainage basin. Stream density data was obtained from Horizon Systems Corporation
388 (http://www.horizon-systems.com/nhdplus/).

389 **Geology**

390 Bedrock is a relative impermeable layer, as the lower boundary of subsurface stormflow in the catchments
391 where soil depth is shallow (Tromp-van Meerveld & McDonnell). The depth to bedrock, as an integrated
392 geologic indicator, was accessed from STATSGO (State Soil Geographic,
393 http://www.soilinfo.psu.edu/index.cgi?soil_data&conus&data_cov&dtb) (Schwarz & Alexander, 1995).
394 The averaged depth to bedrock for each catchment was calculated for further analysis.

4   Results of the Bruntland Burn

4.1   Topography analysis

397 The generated HAND map, derived also from the DEM, is shown in Figure 6, with HAND values ranging
398 from 0m to 234m. Based on the HAND map, we can derive the S_u-A_s curve (Figure 8) by analyzing the
399 HAND map with the method in Section 2.3. The TWI map of the BB (Figure 6) was generated from its DEM.
400 Overall, the TWI map, ranging from -0.4 to 23.4, mainly differentiates the valley bottom areas with the
401 highest TWI values from the steeper slopes. This is probably caused by the fine resolution of the DEM map
402 in 2 m, as previous research found that the sensitivity of TWI to DEM resolution (Sørensen and Seibert,
403 2007). From the TWI map, the frequency distribution function and the accumulative frequency
404 distribution function can be derived (Figure 8), with one unit of TWI as interval.

4.2   Model performance

406 It is found that all the three models (HBV, TOPMODEL, and HSC) can perform well in reproducing the
407 observed hydrograph (Figure 9). The I_{KGE} of the three models are all around 0.66 in calibration, which is
408 largely in line with other studies from the BB (Birkel et al, 2010; 2014). And the I_{KGL} are 0.76, 0.72 and 0.74
409 for HSC, HBV and TOPMODEL respectively in calibration. While in validation, I_{KGE} of the three models are
410 also around 0.66, while I_{KGL} are 0.75, 0.70 and 0.65 for the three models. Since the measured rainfall-
411 runoff time series only lasts from 2008 to 2014, which is too short to estimate the S_{R20y} (proxy for S_{uMax})
412 by MCT approach (which needs long-term hydro-meteorological observation data,) the HSC-MCT model
413 was not applied to this catchment.

414   Figure 8 shows the calibrated power curve by HBV (averaged beta=0.98) with the S_u-A_s curve obtained
415   from the HSC module. We found the two curves are largely comparable, especially while the relative soil
416   moisture is low. This result demonstrates that for the BB catchment with glacial drift deposits and
417   combined terrain of steep and rolling hillslopes and over-widened valley bottoms, the HBV power curve
418   can essentially be derived from the S_u-A_s curve of HSC module merely by topographic information without
419   calibration.

420   The normalized relative soil moisture of the three model simulations are presented in Figure 9. Their
421   temporal fluctuation patterns are comparable. Nevertheless, the simulated soil moisture by TOPMODEL
422   has larger variation, compared with HBV and HSC (Figure 9).

4.3   Contributing area simulation

424   The observed saturation area and the simulated contributing area from both TOPMODEL and the HSC are
425   shown in Figure 7, 9, 10. We found although both modules overestimated the saturated areas, they can
426   capture the temporal variation. For example, the smallest saturated area both observed and simulated
427   occurred on July-02-2008, and the largest saturated area both occurred on January-21-2009. Comparing
428   the estimated contributing area of TOPMODEL with the HSC module, we found the results of the HSC
429   correlates better (R^2=0.60, I_{KGE}=-3.0) with the observed saturated areas than TOPMODEL (R^2=0.50, I_{KGE}=-
430   3.4) (Figure 10). For spatial patterns, the HSC contributing area is located close to the river network and
431   reflects the spatial pattern of observed saturated area. While TOPMODEL results are more scattered,
432   probably due to the sensitivity of TWI to DEM resolution (Figure 7). The HSC is more discriminating in
433   terms of less frequently giving an unrealistic 100% saturation and retaining unsaturated upper hillslopes.

5   Results from the MOPEX catchments

5.1   Topography analysis of the Contiguous US and 323 MOPEX catchments

436   To delineate the TWI map for the CONUS, the depressions of the DEM were firstly filled with a threshold
437   height of 100m (recommended by Esri). The TWI map of the CONUS is produced (Figure S1). Based on the
438   TWI map of the CONUS, we clipped the TWI maps for the 323 MOPEX catchments with their catchment
439   boundaries. And then the TWI frequency distribution and the accumulated frequency distribution of the
440   323 MOPEX catchments (Figure S2), with one unit of TWI as interval, were derived based on the 323 TWI
441   maps.

442   In Figure 11, it is shown that the regions with large HAND values are located in Rocky Mountains and

443   Appalachian Mountains, while the Great Plains has smaller HAND values. The Great Basin, especially in

444   the Salt Lake Desert, has small HAND values, illustrating its low elevation above the nearest drainage,

445   despite a high elevation above sea level. From the CONUS HAND map, we clipped the HAND maps for the

446   323 MOPEX catchments with their catchment boundaries. We then plot their HAND-area curves, following

447   the procedures of I and II in Section 2.2. Figure 12a shows the normalized HAND profiles of the 323

448   catchments.

449   Based on the HAND profiles and the Step III in Section 2.2, we derived the normalized storage capacity

450   distribution for all catchments (Figure 12b). Subsequently, the root zone moisture and saturated area

451   relationship (A_s-S_u) can be plotted by the method in Step IV of Section 2.2. Lastly, reversing the curve of

452   A_s-S_u to S_u-A_s relation (Figure 12c), the latter one can be implemented to simulate runoff generation by

453   soil moisture. Figure 12c interestingly shows that in some catchments, there is almost no threshold

454   behavior between rainfall and runoff generation, where the catchments are covered by large areas with

455   low HAND values and limited storage capacity. Therefore, when rainfall occurs, wetlands response quickly

456   and generate runoff without a precipitation–discharge threshold relationship characteristic of areas with

457   higher moisture deficits. This is similar to the idea of FLEX-Topo where the storage capacity is distinguished

458   between wetlands and hillslopes, and on wetlands, with low storage capacity, where runoff response to

459   rainfall is almost instantaneous.

460   ## 5.2   Model performance

461   Overall, the performance of the two benchmark models, i.e. HBV and TOPMODEL, for the MOPEX data

462   (Figure 13) is comparable with the previous model comparison experiments, conducted with four rainfall-

463   runoff models and four land surface parameterization schemes (Duan et al., 2006; Kollat et al., 2012; Ye

464   et al., 2014). The median value of I_{KGE} of the HBV type model is 0.61 for calibration in the 323 catchments

465   (Figure 13), and averaged I_{KGE} in calibration is 0.62. In validation, the median and averaged values of I_{KGE}

466   are kept the same as calibration. The comparable performance of models in calibration and validation

467   demonstrates the robustness of benchmark models and the parameter optimization algorithm (i.e.

468   MOSCEM-UA). The TOPMODEL improves the median value of I_{KGE} from 0.61 (HBV) to 0.67 in calibration,

469   and from 0.61 (HBV) to 0.67 in validation. But the averaged values of I_{KGE} for TOPMODEL are slightly

470   decreased from 0.62 (HBV) to 0.61 in both calibration and validation. The HSC module, by involving the

471   HAND topographic information without calibrating the β parameter, improves the median value of I_{KGE} to

472   0.68 for calibration and 0.67 for validation. The averaged values of I_{KGE} in both calibration and validation

473   are also increased to 0.65, comparing with HBV (0.62) and TOPMODEL (0.61). Furthermore, Figure 13

474   demonstrates that, comparing with the benchmark HBV and TOPMODEL, not only the median and

475   averaged values were improved by the HSC module, but also the 25th and 75th percentiles and the lower

476   whisker end, all have been improved. The performance gains on baseflow (I_{KGL}) have been investigated

477   and shown in the supplementary figure S3. These results indicate the HSC module improved model

478   performance to reproduce hydrograph for both peak flow (I_{KGE}) and baseflow (I_{KGL}).

479   Additionally, for HSC-MCT model, the median I_{KGE} value is improved from 0.61 (HBV) to 0.65 in calibration,

480   and from 0.61 (HBV) to 0.64 in validation, but not as well performed as TOPMODEL (0.67 for calibration

481   and validation). For the averaged I_{KGE} values, they were slightly reduced from 0.62 (HBV) and 0.61

482   (TOPMODEL) to 0.59 for calibration and validation. Although the HSC-MCT did not perform as well as the

483   HSC module, considering there is no free parameters to calibrate, the median I_{KGE} value of 0.64 (HBV is

484   0.61) and averaged I_{KGE} of 0.59 (TOPMODEL is 0.61) are quite acceptable. In addition, the 25th and 75th

485   percentiles and the lower whisker end of the HSC-MCT model are all improved compared to the HBV

486   model. Moreover, the largely comparable results between the HSC and the HSC-MCT modules

487   demonstrate the feasibility of the MCT method to obtain the S_{uMax} parameter and the potential for HSC-

488   MCT to be implemented in prediction of ungauged basins.

489   Figure 14 shows the spatial comparisons of the HSC and HSC-MCT models with the two benchmark models.

490   We found that the HSC performs "equally well" as HBV (the difference of I_{KGE} in validation ranges -0.1 ~

491   0.1) in 88% catchments, and in the remaining 12% of the catchments the HSC outperforms HBV (the

492   improvement of I_{KGE} in validation is larger than 0.1). In not a single catchment did the calibrated HBV

493   outperform the HSC. Comparing the HSC model with TOPMODEL, we found in 91% of the catchments that

494   the two models have approximately equal performance. In 8% of the catchments, the HSC model

495   outperformed TOPMODEL. Only in 1% of the catchments (two in the Appalachian Mountains and one in

496   the Rocky Mountains in California), TOPMODEL performed better.

497   In order to further explore the impact of catchment characteristics on model performance, we used

498   topography (averaged HAND, averaged slope, and averaged elevation), soil (K-factor), land cover (forest

499   area proportion), climate (aridity index), stream density, and geology (depth to rock) information to test

500   the impact of catchment features on model performance. Table 4 clearly shows that compared with HBV,

501   the 39 catchments with better performance have lower HAND values (37m), more gentle slopes (4.0

502   degree), and smaller forest area (22%); while the elevation, K-factor, aridity index, stream density and

503   depth to rock are almost similar. Also, in the catchments where HSC outperformed TOPMODEL, the

504   catchments have smaller HAND (27m), more gentle slopes (3.6 degree), moderate elevation (469 m), less

505   forest proportion (14%), and more arid climate (aridity index is 1.3). TOPMODEL performs better in only

506   three catchments with larger HAND (193m), steeper slopes (13.5 degree), higher elevation (740 m), more

507   humid climate (aridity index is 0.8), and larger depth to rock (333 cm). In summary, the HSC showed better

508   performance in catchments with gentle topography and more arid climate.

509   Without calibration of S_{uMax}, as expected, the performance of HSC-MCT module slightly deteriorates

510   (Figure 13). In comparison with HBV, the outperformed percentage reduced from 12% (HSC) to 4% (HSC-

511   MCT), the approximately equal-well simulated catchments dropped from 88% to 79%, and the inferior

512   performance increased from 0% to 17%. Also, in comparison with TOPMODEL, the better performance

513   dropped from 8% (HSC) to 7% (HSC-MCT), the approximately equal catchments reduced from 91% to 72%,

514   and the inferior performance increased from 1% to 21%. The inferiority of the HSC-MCT model is probably

515   caused by the uncertainty of the MCT method for different ecosystems which have different survival

516   strategies and use different return periods to bridge critical drought periods. By using ecosystem

517   dependent return periods, this problem could be reduced (Wang-Erlandsson et al., 2016).

518   To further explore the reason for the better performance of the HSC approach, we selected the 08171000

519   catchment in Texas (Figure 14), in which both the HSC module and the HSC-MCT module outperformed

520   the two benchmark modules to reproduce the observed hydrograph (Figure S4). The HBV model

521   dramatically underestimated the peak flows, with I_{KGE} as 0.54, while TOPMODEL significantly

522   overestimated the peak flows, with I_{KGE} as 0.30. The HSC-MCT model improved the I_{KGE} to 0.71, and the

523   HSC model further enhanced I_{KGE} to 0.74.

524   Since the modules of interception, evaporation and routing are identical for the four models, the runoff

525   generation modules are the key to understand the difference in model performance. Figure S5 shows the

526   HBV β curve and the S_u-A_s curve of the HSC model, as well the TWI frequency distribution. We found that

527   with a given S_u/S_{uMax}, the HBV β function generates less contributing area than the HSC model, which

528   explains the underestimation of the HBV model. In contrast, TOPMODEL has a sharp and steep

529   accumulated TWI frequency curve. In particular, the region with TWI=8 accounts for 40% of the catchment

530   area, and over 95% of the catchment areas are within the TWI ranging from 6 to 12. This indicates that

531   even with low soil moisture content (S_u/S_{uMax}), the contributing area by TOPMODEL is relatively large,

532   leading to the sharply increased peak flows for all rainfall events.

6   Discussion

6.1   Rainfall-runoff processes and topography

We applied a novel approach to derive the relationship between soil moisture storage and the saturated area from HAND. The areas with relatively low HAND values are saturated earlier than areas with higher HAND values, due to the larger storage capacity in higher HAND locations. The outperformance of the HSC over the benchmark HBV and TOPMODEL in gentle sloping catchments indicates that the HSC module likely has a higher realism than the calibrated HBV beta-function and the TWI of TOPMODEL in these regions. Very interestingly, Fan et al., (2017) presented an ecological observation in global scale, and revealed the systematic variation of rooting depth along HAND (Fig.1, in Fan et al., 2017). Since rooting depth can be translated to root zone storage capacity through combination with soil plant-available water (Wang-Erlandsson et al., 2016). This large sample dataset, from ecological perspective, provides a strong support for the assumption of the HSC model on gentle slopes, i.e. the increase of root zone storage capacity with HAND. More interestingly, on excessively drained uplands, rooting depth does not follow the same pattern, with shallow depth and limited to rain infiltration (Fig.1, in Fan et al., 2017). This could explain the inferior performance of HSC model to TOPMODEL in three MOPEX catchments with excessively drained uplands (larger HAND, steeper slope, higher elevation, and deeper depth to rock), where Hortonian overland flow is likely the dominant mechanism, and the HSC assumption likely does not work well. This indicates that comparing with TWI, the HAND is closer to catchment realism distinguishing hydrological similarity in gentle topography catchments. The HSC module assumes SEF as the dominant mechanism. But since in a real catchment different runoff generating processes may act simultaneously in different environments (McDonnell, 2013; Hrachowitz and Clark, 2017). Such SEF dominated catchments, or parts thereof, are typically characterized by a subdued relief and thus gently sloping. In steeper catchments, where the groundwater table is deeper and thus more additional water can be stored in the soil, another conceptual parametrisation would be appropriate.

The FLEX-Topo model (Savenije, 2010) also uses HAND as a topographic index to distinguish between landscape-related runoff processes and has both similarity and differences with the HSC model. The results of the HSC model illustrate that the riparian areas are more prone to be saturated, which is consistent with the concept of the FLEX-Topo model. Another important similarity of the two models is their parallel model structure. In both models it is assumed that the upslope area has larger storage capacity, therefore the upper land generates runoff less and later than the lower land. In other words, in most cases, the local storage is saturated due to the local rainfall, instead of flow from upslope. The most

564 obvious difference between the HSC and the FLEX-Topo is the approach towards discretization of a
565 catchment. The FLEX-Topo model classifies a catchment into various landscapes, e.g. wetlands, hillslopes
566 and plateau. This discretization method requires threshold values to classify landscapes, i.e. threshold
567 values of HAND and slope, which leads to fixed and time-independent proportions of landscapes. The HSC
568 model does not require landscape classification, which reduced the subjectivity in discretization and
569 restricted the model complexity, as well as simultaneously allowing the fluctuation of contributing areas
570 (termed as wetlands in FLEX-Topo).

6.2 Catchment heterogeneity and simple models

572 Catchments exhibit a wide array of heterogeneity and complexity with spatial and temporal variations of
573 landscape characteristics and climate inputs. For example, the Darcy-Richards equation approach is often
574 consistent with point-scale measurements of matrix flow, but not for preferential flow caused by roots,
575 soil fauna and even cracks and fissures (Beven and Germann, 1982; Zehe and Fluehler, 2001; Weiler and
576 McDonnell, 2007). As a result, field experimentalists continue to characterize and catalogue a variety of
577 runoff processes, and hydrological and land surface modelers are developing more and more complicated
578 models to involve the increasingly detailed processes (McDonnell et al., 2007). However, there is still no
579 compelling evidence to support the outperformance of sophisticated "physically-based" models in terms
580 of higher equifinality and uncertainty than the simple lumped or semi-distributed conceptual models in
581 rainfall-runoff simulation (Beven, 1989; Orth et al., 2015).

582 But evidence is mounting that a catchment is not a random assemblage of different heterogeneous parts
583 (Sivapalan, 2009; Troch et al., 2013; Zehe et al., 2013), and conceptualising heterogeneities does not
584 require complex laws (Chase, 1992; Passalacqua et al., 2015). Parsimonious models (e.g. Perrin et al.,
585 2003), with empirical curve shapes, likely result in good model performance. Parameter identifiability in
586 calibration is one of the reasons. However, the physical rationale of these parsimonious models is still
587 largely unknown lacking a physical explanation to interpret these empirical curves described by
588 mathematical functions (e.g. Equation 3 in Perrin et al., 2003).

589 The benefits of the new HSC module are two-fold. From a technical point of view, the HSC allows us to
590 make Prediction in Ungauged Basins without calibrating the beta parameter in many conceptual
591 hydrological models. Furthermore, the HSC module, from a scientific point of view, provides us with a new
592 perspective on the linkage between the spatial distribution patterns of root zone storage capacity (long-
593 term ecosystem evolution) with associated runoff generation (event scale rainfall-runoff generation).

594 Asking questions of "why" rather than "what" likely leads to more useful insights and a new way forward
595 (McDonnell et al., 2007). The HSC module provides us with a rationale from an ecological perspective to
596 understand the linkage and mechanism between large-sample hillslope ecological observations and the curve
597 of root zone storage capacity distribution (Figure 1, 2, 3). Catchment is a geomorphological and even an
598 ecological system whose parts are related to each other probably due to catchment self-organization and
599 evolution (Sivapalan and Blöschl, 2015; Savenije and Hrachowitz, 2017). This encourages the hope that
600 simplified concepts may be found adequate to describe and model the operation of the basin runoff
601 generation process. It is clear that topography, with fractal characteristic (Rodriguez-Iturbe and Rinaldo,
602 1997), is often the dominant driver of runoff, as well as being a good integrated indicator for vegetation
603 cover (Gao et al., 2014b), rooting depth (Fan et al., 2017), root zone evaporation and transpiration deficits
604 (Maxwell and Condon, 2016), soil properties (Seibert et al., 2007), and even geology (Rempe and Dietrich,
605 2014; Gomes, 2016). Therefore, we argue that increasingly detailed topographic information is an
606 excellent integrated indicator allowing modelers to continue systematically represent heterogeneities and
607 simultaneously reduce model complexity. The model structure and parameterization of both HSC and
608 TOPMODEL are simple, but not over simplified, as they capture likely the most dominant factor controlling
609 runoff generation, i.e. the spatial heterogeneity of storage capacity. Hence, this study also sheds light on
610 the possibility of moving beyond heterogeneity and process complexity (McDonnell et al., 2007), to
611 simplify them into a succinct and *a priori* curve by taking advantage of catchment self-organization
612 probably caused by co-evolution or the principle of maximum entropy production (Kleidon and Lorenz,
613 2004).

6.3   Implications and limitation

615 The calibration-free HSC-MCT runoff generation module enhances our ability to predict runoff in
616 ungauged basins. PUB is probably not a major issue in the developed world, with abundant of
617 comprehensive measurements in many places, but for the developing world it requires prediction with
618 sparse data and fragmentary knowledge. Topographic information with high spatial resolution is freely
619 available globally, allowing us to implement the HSC model in global scale studies. In addition, thanks to
620 the recent development, testing, and validation of remote sensing evaporation products in large spatial
621 scale (e.g. Anderson et al., 2011; Hu and Jia, 2015), the S_{uMax} estimation has become possible without in
622 situ hydro-meteorological measurements (Wang-Erlandsson et al., 2016). These widely-accessible
623 datasets make the global-scale implementation of HSC-MCT module promising.

624 Although the new modules perform well in the BB and the MOPEX catchments, we do not intend to

625 propose "a model fits all". The assumption of HSC, to some extent, is supported by large-sample ecological

626 field observation (Fan et al., 2017), but it never means the A_s-S_u curve of HSC can perfectly fit the other

627 existing curves (e.g. HBV and TOPMODEL). Unify all model approaches into one framework is the objective

628 of several pioneer works (e.g. Clark, et al., 2010; Fenicia et al., 2011), but out of the scope of this study.

629 Moreover, while estimating the runoff coefficient by the A_s-S_u relation, rainfall in the early time may cause

630 the increase of S_u/S_{uMax} and runoff coefficient (Moore, 1985; Wang, 2018). Therefore, neglecting this

631 influence factor, HBV (Equation 1), TOPMODEL (Equation 2-4) and HSC (Equation 5-6) theoretically

632 underestimate the runoff coefficient, which needs to be further investigated.

633 Finally, we should not ignore the limitations of the new module, although it has better performance and

634 modelling consistency. 1) The threshold area for the initiating a stream was set as a constant value for the

635 entire CONUS, but the variation of this value in different climate, geology and landscape classes

636 (Montgomery and Dietrich, 1989; Helmlinger et al., 1993; Colombo et al., 2007; Moussa, 2008) needs to

637 be future investigated. 2) The discrepancy between observed and simulated saturation area needs to be

638 further investigated, by utilizing more advanced field measurement and simultaneously refining the

639 model assumption. To our understanding, there are two interpretations. Firstly, the overestimation of the

640 HSC model is possibly because two runoff generation mechanisms – SOF and the SSF occur at the same

641 time. However, the saturated area observed by the "squishy boot" method (Ali et al., 2013), probably only

642 distinguished the areas where SOF occurred. Subsurface stormflow, also contributing to runoff, cannot be

643 observed by the "squishy boot" method. Thus, this mismatch between simulation and observation

644 probably leads to this saturated area overestimation. The second interpretation might be the different

645 definition of "saturation". The observed saturated areas are places where 100% of soil pore volume is

646 filled by water. But the modelled saturation areas are located where soil moisture is above field capacity,

647 and not necessarily 100% filled with water, which probably also results in the overestimation of saturated

648 areas. Interestingly, in theory the observed saturated area should be within the simulated contributing

649 area, due to the fact that the saturated soil moisture is always larger than field capacity. From this point

650 of view, the observed saturated area is smaller and within the contributing area simulated by HSC, but

651 TOPMODEL missed this important feature. 4) Only the runoff generation module is calibration free, but

652 the interception and response routines still rely on calibration. Although we kept the interception and

653 response routine modules the same for the four models, the variation of other calibrated parameters (i.e.

654 S_{iMax}, D, K_f, K_s, T_{lagF}) may also influence model performance in both calibration and validation. 5) The

655 computational cost of the HSC is more expensive than HBV, and similar to TOPMODEL, due to the cost of

656 preprocessed topographic analysis. But once the S_u-A_s curve is completed, the computation cost is quite

657 comparable with HBV.

7   Summary and conclusions

659 In this study, we developed a simple and calibration-free hydrological module (HAND-based Storage

660 Capacity curve, HSC) based on a relatively new topographic index (HAND), which is not only an excellent

661 physically-based indictor for the hydraulic gradient, but also represents the spatial distribution of root

662 zone storage capacity supported by large-sample ecological observations. Based on HAND spatial

663 distribution pattern, the soil moisture (S_u) - saturated area (A_s) relation for each catchment was derived,

664 which was used to estimate the A_s of specific rainfall event based on continuous calculation of S_u.

665 Subsequently, based on the S_u-A_s relation, the HSC module was developed. Then, applying the mass curve

666 technique (MCT) approach, we estimated the root zone storage capacity (S_{uMax}) from observable hydro-

667 climatological and vegetation data, and coupled it with HSC to create the calibration-free HSC-MCT

668 module. The HBV and TOPMODEL were used as two benchmarks to test the performance of HSC and HSC-

669 MCT on both hydrograph simulation and ability to reproduce the contributing area, which was measured

670 for different hydrometeorological conditions in the Bruntland Burn catchment in Scotland. Subsequently,

671 323 MOPEX catchments in the US were used as a large-sample hydrological study to further validate the

672 effectiveness of our proposed runoff generation modules.

673 In the BB exploratory study, we found that the HSC, HBV and TOPMODEL performed comparably well to

674 reproduce the observed hydrograph. Comparing the estimated contributing area of TOPMODEL with the

675 HSC module, we found that HSC module performed better to reproduce saturated area variation, in terms

676 of the correlation coefficient and spatial patterns. This likely indicates that HAND maybe a better indicator

677 to distinguish hydrological similarity than TWI.

678 For the 323 MOPEX catchments, HSC improved the averaged validation value of I_{KGE} from 0.62 (HBV) and

679 0.61 (TOPMODEL) to 0.65. In 12% of the MOPEX catchments, the HSC module outperforms HBV, and in

680 not a single catchment did the calibrated HBV outperform the HSC. Comparing with TOPMODEL, the HSC

681 outperformed in 8% of the catchments, and in only 1% of catchments TOPMODEL has a better

682 performance. Interestingly, we found that the HSC module showed better performance in the catchments

683 with gentle topography, less forest cover, and larger aridity index. Not surprisingly, the I_{KGE} of HSC-MCT

684 model was slightly reduced to 0.59, due to the non-calibrated S_{uMax}, but still comparably well performed

685 as HBV (0.62) and TOPMODEL (0.61). This illustrates the robustness of both the HSC approach to derive

686   the spatial distribution of the root zone storage capacity (β) and the efficiency of the MCT method to

687   estimate the root zone storage capacity (S_{uMax}).

688

689   **Acknowledgement:**

690   This study was supported by National Natural Science Foundation of China (41801036), National Key R&D

691   Program of China (2017YFE0100700), the Key Program of National Natural Science Foundation of China

692   (No. 41730646), and Key Laboratory for Mountain Hazards and Earth Surface Process, Institute of

693   Mountain Hazards and Environment, Chinese Academy of Sciences (KLMHESP-17-02).

694

695   **Author contributions:**

696   H.G. and H.H.G.S. designed research; H.G. performed research; C.B., C.S., D.T and H.G. provided data,

697   among which the dynamics of the saturation areas data in the BB was provided by C.B. C.S., and D.T.; H.G.

698   analysed data; C.B. was involved in the interpretation of some of the modelling work in the BB; H.G. M.H,

699   and H.H.G.S. wrote the paper; CS and DT extensively edited the paper, and provided substantial comments

700   and constructive suggestions for scientific clarification.

701

702 References:

703   Anderson, M. C., Kustas, W. P., Norman, J. M., Hain, C. R., Mecikalski, J. R., Schultz, L., González-Dugo, M.

704   P., Cammalleri, C., D'Urso, G., Pimstein, A., and Gao, F.: Mapping daily evapotranspiration at field to

705   continental scales using geostationary and polar orbiting satellite imagery, Hydrol. Earth Syst. Sci., 15,

706   223–239, doi:10.5194/hess-15-223-2011, 2011.

707   Andréassian V, Bourgin F, Oudin L, Mathevet T, Perrin C, Lerat J, Coron L, Berthet L.: Seeking genericity in

708   the selection of parameter sets: Impact on hydrological model efficiency. Water Resources Research 50

709   (10): 8356–8366, 2014.

710   Bergström S, Forsman A.: Development of a conceptual deterministic rainfall-runoff model. Hydrology

711   Research 4 (3): 147–170, 1973.

712   Bergström S, Lindström G.: Interpretation of runoff processes in hydrological modelling—experience from

713   the HBV approach. Hydrological Processes 29 (16): 3535–3545, 2015.

714   Beven K.: Robert E. Horton's perceptual model of infiltration processes. Hydrological Processes 18 (17):

715   3447–3460 DOI: 10.1002/hyp.5740, 2004.

716   Beven K, Freer J.: A dynamic TOPMODEL. Hydrological Processes 15 (10): 1993–2011 DOI: 10.1002/hyp,

717   2001.

718   Beven K. 1993. Prophecy, reality and uncertainty in distributed hydrological modelling. Advances in Water

719   Resources 16 (1): 41–51 DOI: http://dx.doi.org/10.1016/0309-1708(93)90028-E

720   Beven K.: Linking parameters across scales: Subgrid parameterizations and scale dependent hydrological

721   models. Hydrological Processes 9 (September 1994): 507–525 DOI: 10.1002/hyp.3360090504.252, 1995.

722   Beven KJ.: Rainfall–Runoff Models: The Primer, 2012.

723   Beven K., Germann P.: Macropores and water-flow in soils. Water Resour. Res. 18, 1311–1325, 1982.

724   Beven KJ, Kirkby MJ.: A physically based, variable contributing area model of basin hydrology. Hydrological

725   Sciences Bulletin 24 (1): 43–69 DOI: 10.1080/02626667909491834, 1979.

726   Beven, K.: Changing ideas in hydrology – the case of physically-based models. J. Hydrol. 105 (1–2), 157–

727   172, 1989.

728   Birkel C, Tetzlaff D, Dunn SM, Soulsby C.: Towards a simple dynamic process conceptualization in rainfall‐

729   runoff models using multi‐criteria calibration and tracers in temperate, upland catchments. Hydrological

730   Processes 24 (3): 260–275, 2010.

731   Birkel, C., Soulsby, C., and Tetzlaff, D.: Conceptual modelling to assess how the interplay of hydrological

732   connectivity, catchment storage and tracer dynamics controls non-stationary water age estimates.

733   Hydrological Processes, DOI: 10.1002/hyp.10414, 2014.

734   Blöschl G.: Runoff prediction in ungauged basins: synthesis across processes, places and scales. Cambridge

735   University Press, 2013.

736   Brooks, R. J., Barnard, H. R., Coulombe, R. & McDonnell, J. J.: Ecohydrologic separation of water between

737   trees and streams in a Mediterranean climate. Nature Geoscience 3, 100–104. DOI: 10.1038/ngeo722,

738   2010.

739   Budyko MI.: Climate and life, 1971.

740   Burt TP, McDonnell JJ.: Whither field hydrology? The need for discovery science and outrageous
741   hydrological hypotheses. Water Resources Research 51 (8): 5919–5928 DOI: 10.1002/2014WR016839,
742   2015.

743   Chase, CG.: Fluvial landsculpting and the fractal dimension of topography. Geomorphology 5 (1): 39–57
744   DOI: http://dx.doi.org/10.1016/0169-555X(92)90057-U, 1992.

745   Clark, MP, Slater, AG, Rupp, DE, Woods, R A., Vrugt, J A., Gupta, H V., Wagener, T, Hay, LE.: Framework for
746   Understanding Structural Errors (FUSE): A modular framework to diagnose differences between
747   hydrological models. Water Resources Research 44: 1–14 DOI: 10.1029/2007WR006735, 2008.

748   Clark, M. P., Kavetski, D. and Fenicia, F.: Pursuing the Method of Multiple Working Hypotheses for
749   Hydrological Modeling. Water Resources Research 47.9: 1–16, 2011.

750   Colombo, R., Vogt, J. V., Soille, P., Paracchini, M. L., de Jager, A.: Deriving river networks and catchments
751   at the European scale from medium resolution digital elevation data. CATENA 70 (3): 296–305 DOI:
752   http://doi.org/10.1016/j.catena.2006.10.001, 2007.

753   Condon, Laura E, and Reed M Maxwell. "Evaluating the Relationship between Topography and
754   Groundwater Using Outputs from a Continental-Scale Integrated Hydrology Model." Water Resources
755   Research 51.8 (2015): 6602–6621.

756   Duan, Q., Schaake, J., Andréassian, V., Franks, S., Goteti, G., Gupta, H. V., Gusev, YM, Habets, F., Hall, A.,
757   Hay, L., Model Parameter Estimation Experiment (MOPEX): An overview of science strategy and major
758   results from the second and third workshops. Journal of Hydrology 320 (1-2): 3–17 DOI:
759   10.1016/j.jhydrol.2005.07.031, 2006.

760   Dunne, T., Black, R.D.: Partial area contributions to Storm Runoff in a Small New England Watershed.
761   Water Resources Research 6 (5): 1296–1311, 1970.

762   Boer-Euser, T., McMillan, H. K., Hrachowitz, M., Winsemius, H. C., and Savenije, H. H. G.: Influence of soil
763   and climate on root zone storage capacity, Water Resour. Res., 52, 2009–2024,
764   doi:10.1002/2015WR018115, 2016.

765 Fan, Y., Miguezmacho, G., Jobbágy, E. G., Jackson, R. B., & Oterocasal, C.: Hydrologic regulation of plant
766 rooting depth. Proceedings of the National Academy of Sciences of the United States of America, 114(40),
767 201712381, 2017.

768 Fenicia, F., Savenije, H.H.G., Matgen, P., Pfister, L.: A comparison of alternative multiobjective calibration
769 strategies for hydrological modeling. Water Resources Research 43 (3): n/a–n/a DOI:
770 10.1029/2006WR005098, 2007.

771 Gao, H., Hrachowitz, M., Schymanski, S.J., Fenicia, F., Sriwongsitanon, N., Savenije, H.H.G.: Climate
772 controls how ecosystems size the root zone storage capacity at catchment scale. Geophysical Research
773 Letters 41 (22): 7916–7923 DOI: 10.1002/2014gl061668, 2014a.

774 Gao, H., Hrachowitz, M., Fenicia, F., Gharari, S., Savenije, H.H.G.: Testing the realism of a topography-
775 driven model (FLEX-Topo) in the nested catchments of the Upper Heihe, China. Hydrology and Earth
776 System Sciences 18 (5): 1895–1915 DOI: 10.5194/hess-18-1895-2014, 2014b.

777 Gao, H., Hrachowitz, M., Sriwongsitanon, N., Fenicia, F., Gharari, S., Savenije, H.H.G.: Accounting for the
778 influence of vegetation and landscape improves model transferability in a tropical savannah region. Water
779 Resources Research 52 (10): 7999–8022 DOI: 10.1002/2016WR019574, 2016.

780 Gao, H., Sabo, J.L, Chen, X., Liu, Z., Yang, Z., Ren, Z., Liu, M.: Landscape heterogeneity and hydrological
781 processes: a review of landscape-based hydrological models. Landscape Ecology, DOI:
782 doi.org/10.1007/s10980-018-0690-4, 2018a.

783 Gao, H., Cai, H., Zheng, D.: Understand the impacts of landscape features on the shape of storage capacity
784 curve and its influence on flood. Hydrology Research. DOI: Hydrology-D-16-00245R3, 2018b.

785 Gao, J., Holden, J., Kirkby, M.: The impact of land-cover change on flood peaks in peatland basins. Water
786 Resources Research 52 (5): 3477–3492 DOI: 10.1002/2015WR017667, 2016.

787 Gharari, S., Hrachowitz, M., Fenicia, F., Savenije, H.H.G.: Hydrological landscape classification:
788 investigating the performance of HAND based landscape classifications in a central European meso-scale
789 catchment. Hydrology and Earth System Sciences 15 (11): 3275–3291 DOI: 10.5194/hess-15-3275-2011,
790 2011.

791 Gharari, S., Hrachowitz, M., Fenicia, F., Gao, H., Savenije, H.H.G.: Using expert knowledge to increase

792 realism in environmental system models can dramatically reduce the need for calibration. Hydrology and

793 Earth System Sciences 18 (12): 4839–4859 DOI: 10.5194/hess-18-4839-2014, 2014.

794 Gharari, S. On the role of model structure in hydrological modeling: Understanding models, PhD

795 dissertation, 2016

796 Gomes, G.J.C., Vrugt, J.A., Vargas, E.A.: Toward improved prediction of the bedrock depth underneath

797 hillslopes: Bayesian inference of the bottom-up control hypothesis using high-resolution topographic data.

798 Water Resources Research 52 (4): 3085–3112 DOI: 10.1002/2015WR018147, 2016.

799 Grabs, T., Seibert, J., Bishop, K., Laudon, H.: Modeling spatial patterns of saturated areas: A comparison

800 of the topographic wetness index and a dynamic distributed model. Journal of Hydrology 373 (1): 15–23,

801 2009.

802 De Groen, M.M., Savenije, H.H.G.: A monthly interception equation based on the statistical characteristics

803 of daily rainfall. Water Resources Research 42 (12): n/a–n/a DOI: 10.1029/2006WR005013, 2006.

804 Gumbel, E. J.: Les valeurs extrêmes des distributions statistiques, Annales de l'institut Henri Poincaré, 5(2),

805 115–158, 1935.

806 Gupta, H. V., Kling, H., Yilmaz, K.K., Martinez, G.F.: Decomposition of the mean squared error and NSE

807 performance criteria: Implications for improving hydrological modelling. Journal of Hydrology 377 (1-2):

808 80–91 DOI: 10.1016/j.jhydrol.2009.08.003, 2009.

809 Hargreaves, G.H., Samani, Z.A.: Reference crop evapotranspiration from temperature. Applied

810 engineering in agriculture 1 (2): 96–99, 1985.

811 Haria, A.H., Shand, P.: Evidence for deep sub-surface flow routing in forested upland Wales: implications

812 for contaminant transport and stream flow generation. Hydrology and Earth System Sciences Discussions

813 8 (3): 334–344, 2004.

814 Harte, J.: Toward a synthesis of the Newtonian and Darwinian worldviews. Physics Today 55 (10): 29–34

815 DOI: 10.1063/1.1522164, 2002.

816 Helmlinger, K.R., Kumar, P., Foufoula-Georgiou, E.: On the use of digital elevation model data for

817 Hortonian and fractal analyses of channel network. Water Resources Research 29: 2599–2613, 1993.

818 Hewlett, J.D.: Soil moisture as a source of base flow from steep mountain watersheds. Southeastern Forest
819 Experiment Station, US Department of Agriculture, Forest Service, 1961.

820 Hewlett, J.D., Troendle, C.A.: Non point and diffused water sources: a variable source area problem. In
821 Watershed Management; Proceedings of a Symposium, 1975.

822 Homer, C. G., Dewitz, J. A., Yang, L., Jin, S., Danielson, P., Xian, G., Coulston, J., Herold, N. D., Wickham, J.
823 D. & Megown, K.: Completion of the 2011 National Land Cover Database for the conterminous United
824 States-representing a decade of land cover change information. Photogrammetric Engineering and
825 Remote Sensing 81, 345–354, 2015.

826 Hooshyar, M., Wang, D., Kim, S., Medeiros, S.C., Hagen, S.C.: Valley and channel networks extraction based
827 on local topographic curvature and k‐means clustering of contours. Water Resources Research 52 (10):
828 8081–8102, 2016.

829 Horton, R.E.: The role of infiltration in the hydrologic cycle. Trans. Am. Geophys. Union 14, 446–460, 1933.

830 Hrachowitz, M., Savenije, H.H.G., Blöschl, G., McDonnell, J.J., Sivapalan, M., Pomeroy, J.W., Arheimer, B.,
831 Blume, T., Clark, M.P., Ehret, U., Fenicia, F., Freer, J.E., Gelfan, A., Gupta, H.V., Hughes, D.A., Hut, R.W.,
832 Montanari, A., Pande, S., Tetzlaff, D., Troch, P.A., Uhlenbrook, S., Wagener, T., Winsemius, H.C., Woods,
833 R.A., Zehe E., & Cudennec, C.: . A decade of Predictions in Ungauged Basins (PUB)—a review. Hydrological
834 Sciences Journal 58 (6): 1198–1255 DOI: 10.1080/02626667.2013.803183, 2013.

835 Hrachowitz, M. and Clark, M. P.: HESS Opinions: The complementary merits of competing modelling
836 philosophies in hydrology, Hydrol. Earth Syst. Sci., 21, 3953-3973, https://doi.org/10.5194/hess-21-3953-
837 2017, 2017.

838 Hu, G. and Jia, L.: Monitoring of evapotranspiration in a semiarid inland river basin by combining
839 microwave and optical remote sensing observations, Remote Sens., 7, 3056–3087,
840 doi:10.3390/rs70303056, 2015.

841 Iorgulescu, I., Jordan, J-P.: Validation of TOPMODEL on a small Swiss catchment. Journal of Hydrology 159
842 (1): 255–273 DOI: http://dx.doi.org/10.1016/0022-1694(94)90260-7, 1994.

843 Kirchner, J.W.: Getting the right answers for the right reasons: Linking measurements, analyses, and
844 models to advance the science of hydrology. Water Resources Research 42 (3): n/a–n/a DOI:
845 10.1029/2005WR004362, 2006.

846 Kleidon, A., Lorenz, R.D.: Non-equilibrium thermodynamics and the production of entropy: life, earth, and
847 beyond. Springer Science & Business Media, 2004.

848 Kollat, J. B., P. M. Reed, and T. Wagener.: When are multiobjective calibration trade‐offs in hydrologic
849 models meaningful?. Water Resources Research 48.3:3520, 2012.

850 Liang, X., Lettenmaier, D.P., Wood, E,F,, Burges, S,J.: A simple hydrologically based model of land surface
851 water and energy fluxes for general circulation models. Journal of Geophysical Research 99 (D7): 14415
852 DOI: 10.1029/94JD00483, 1994.

853 Liu, D., Tian, F., Hu, H., Hu, H.: The role of run-on for overland flow and the characteristics of runoff
854 generation in the Loess Plateau, China. Hydrological Sciences Journal 57 (6): 1107–1117 DOI:
855 10.1080/02626667.2012.695870, 2012.

856 Maxwell, R. M., and Condon, L. E.: Connections between Groundwater Flow and Transpiration Partitioning.
857 Science 353.6297: 377 LP − 380, 2016.

858 McDonnell, J.J., Sivapalan, M., Vaché, K., Dunn, S., Grant, G., Haggerty, R., Hinz, C., Hooper, R., Kirchner,
859 J., Roderick, M.L., Selker, J. and Weiler, M.: Moving beyond heterogeneity and process complexity: A new
860 vision for watershed hydrology. Water Resources Research 43 (7): n/a–n/a DOI: 10.1029/2006WR005467,
861 2007.

862 McDonnell, J.J.: Are all runoff processes the same? Hydrological Processes 27 (26): 4103–4111 DOI:
863 10.1002/hyp.10076, 2013.

864 Merz, R., Blöschl, G.: Regionalisation of catchment model parameters. Journal of Hydrology 287 (1-4): 95–
865 123 DOI: 10.1016/j.jhydrol.2003.09.028, 2004.

866 Milly, P. C. D.: Climate, soil water storage, and the average annual water balance, Water Resour. Res.,
867 30(7), 213–2156, 1994.

868 Molenat, J., Gascuel-Odoux, C., Ruiz, L., Gruau, G.: Role of water table dynamics on stream nitrate export
869 and concentration in agricultural headwater catchment (France). Journal of Hydrology 348 (3): 363–378,
870 2008.

871 Molénat, J., Gascuel‐Odoux, C., Davy, P., Durand, P.: How to model shallow water‐table depth
872 variations: the case of the Kervidy‐Naizin catchment, France. Hydrological Processes 19 (4): 901–920,
873 2005.

874 Montgomery, D.R., Dietrich, W.E.: Source areas, drainage density, and channel initiation. Water Resources
875 Research 25 (8): 1907–1918, 1989.

876 Moore, R. J.: The probability-distributed principle and runoff production at point and basin scales, Hydrol.
877 Sci. J., 30, 273-297, 1985.

878 Moussa, R.: Effect of channel network topology, basin segmentation and rainfall spatial distribution on
879 the geomorphologic instantaneous unit hydrograph transfer function. Hydrological Processes 22 (3): 395–
880 419 DOI: 10.1002/hyp.6612, 2008.

881 Moussa, R.: Definition of new equivalent indices of Horton-Strahler ratios for the derivation of the
882 Geomorphological Instantaneous Unit Hydrograph. Water Resources Research 45 (9): n/a–n/a DOI:
883 10.1029/2008WR007330, 2009.

884 Nobre, A. D, Cuartas, L. A., Hodnett, M., Rennó, C.D., Rodrigues, G., Silveira, A., Waterloo, M., Saleska, S.:
885 Height Above the Nearest Drainage - a hydrologically relevant new terrain model. Journal of Hydrology
886 404 (1-2): 13–29 DOI: 10.1016/j.jhydrol.2011.03.051, 2011.

887 Orth, R., Staudinger, M., Seneviratne, S.I., Seibert, J., Zappa, M.: Does model performance improve with
888 complexity? A case study with three hydrological models. Journal of Hydrology 523: 147–159 DOI:
889 http://doi.org/10.1016/j.jhydrol.2015.01.044, 2015.

890 Passalacqua, P., Belmont, P., Staley, D.M., Simley, J.D., Arrowsmith, J.R., Bode, C.A., Crosby, C., DeLong,
891 S.B., Glenn, N.F., Kelly, S.A., Lague, D., Sangireddy, H., Schaffrath, K., Tarboton, D. G., Wasklewicz, T.,
892 Wheaton, J. M.: Analyzing high resolution topography for advancing the understanding of mass and
893 energy transfer through landscapes: A review. Earth-Science Reviews 148: 174–193 DOI:
894 http://doi.org/10.1016/j.earscirev.2015.05.012, 2015.

895 Pelletier, J.D., Barron-Gafford, G.A., Breshears, D.D., Brooks, P.D., Chorover, J., Durcik, M., Harman, C.J.,
896 Huxman, T.E., Lohse, K.A., Lybrand, R., Meixner, T., McIntosh, J. C., Papuga, S. A., Rasmussen, C., Schaap,
897 M., Swetnam, T. L., and Troch, P. A.: Coevolution of nonlinear trends in vegetation, soils, and topography
898 with elevation and slope aspect: A case study in the sky islands of southern Arizona. Journal of Geophysical
899 Research: Earth Surface 118 (2): 741–758 DOI: 10.1002/jgrf.20046, 2013.

900 Perrin, C., Michel, C., Andréassian, V.: Does a large number of parameters enhance model performance?
901 Comparative assessment of common catchment model structures on 429 catchments. Journal of
902 Hydrology 242 (3-4): 275–301 DOI: 10.1016/S0022-1694(00)00393-0, 2001.

903 Perrin, C., C. Michel, and V. Andre´assian: Improvement of a parsimonious model for streamflow
904 simulation, J. Hydrol., 279, 275– 289, 2003.

905 Ponce, V. M., and Hawkins, R. H.: Runoff curve number: Has it reached maturity?, J. Hydrol. Eng., 1(1), 11–
906 19, 1996.

907 Rempe, D. M., and Dietrich, W. E.: A bottom-up control on fresh-bedrock topography under landscapes,
908 Proc. Natl. Acad. Sci. U. S. A., 111(18), 6576–6581, doi:10.1073/pnas.1404763111, 2014.

909 Renard, K. G., Yoder, D. C., Lightle, D. T. & Dabney, S. M. Universal soil loss equation and revised universal
910 soil loss equation. Handbook of Erosion Modelling 8, 135–167, 2011.

911 Rennó, C.D., Nobre, A.D., Cuartas, L.A., Soares, J.V., Hodnett, M.G., Tomasella, J., Waterloo, M. HAND, a
912 new terrain descriptor using SRTM-DEM; mapping terra-firme rainforest environments in Amazonia.
913 Remote Sensing of Environment 112, 3469–3481, 2008.

914 Rodriguez-Iturbe, I., and A. Rinaldo, Fractal River Basins: Chance and Self-Organization, Cambridge Univ.
915 Press, 547 pp., New York, 1997.

916 Samaniego, L., Kumar, R., Attinger, S.: Multiscale parameter regionalization of a grid-based hydrologic
917 model at the mesoscale. Water Resources Research 46 (5): n/a–n/a DOI: 10.1029/2008WR007327, 2010.

918 Savenije, H. H. G.: HESS Opinions "Topography driven conceptual modelling (FLEX-Topo)", Hydrol. Earth
919 Syst. Sci., 14, 2681–2692, doi:10.5194/hess-14-2681-2010, 2010.

920 Savenije, H.H.G., Hrachowitz, M.: HESS Opinions 'Catchments as meta-organisms – a new blueprint for
921 hydrological modelling'. Hydrol. Earth Syst. Sci. 21 (2): 1107–1116 DOI: 10.5194/hess-21-1107-2017, 2017.

922 Schaake, J., Cong, S., and Duan, Q.: The US MOPEX data set, IAHS Publ., 307, 9, 2006.

923 Schwarz, G. E. & Alexander, R. B. State Soil Geographic (STATSGO) Data Base for the Conterminous United
924 States. Open File report 95-449, US Geological Survey, Washington, DC, 1995.

925 Seibert, J., Stendahl, J., Sørensen, R.: Topographical influences on soil properties in boreal forests.
926 Geoderma 141 (1-2): 139–148 DOI: 10.1016/j.geoderma.2007.05.013, 2007.

927 Shao, W., Su, Y., and Langhammer, J.: Simulations of coupled non-isothermal soil moisture transport and
928 evaporation fluxes in a forest area. Journal of Hydrology and Hydromechanics, 65, 410–425, 2018

929 Shand, P., Haria, A.H., Neal, C., Griffiths, K., Gooddy, D., Dixon, A.J., Hill, T., Buckley, D.K., Cunningham, J.:
930 Hydrochemical heterogeneity in an upland catchment: further characterisation of the spatial, temporal
931 and depth variations in soils, streams and groundwaters of the Plynlimon forested catchment, Wales.
932 Hydrology and Earth System Sciences 9 (6): 621–644, 2005.

933 Sørensen, R., Seibert, J.: Effects of DEM resolution on the calculation of topographical indices: TWI and its
934 components. Journal of Hydrology 347 (1): 79–89 DOI: http://dx.doi.org/10.1016/j.jhydrol.2007.09.001,
935 2007.

936 Sivapalan, M., Woods, R.A., Kalma, J.D.: Variable bucket representation of TOPMODEL and investigation
937 of the effects of rainfall heterogeneity. Hydrological processes 11 (9): 1307–1330, 1997.

938 Sivapalan, M., Takeuchi, K., Franks, S.W., Gupta, V.K., Karambiri, H., Lakshmi, V., Liang, X., McDonnell, J.J.,
939 Mendiondo, E.M., O'Connell, P.E., Oki, T., Pomeroy, J. W., Schertzer, D., Uhlenbrook, S., Zehe, E.: IAHS
940 Decade on Predictions in Ungauged Basins (PUB), 2003–2012: Shaping an exciting future for the
941 hydrological sciences. Hydrological Sciences Journal 48 (6): 857–880 DOI: 10.1623/hysj.48.6.857.51421,
942 2003.

943 Sivapalan, M.: The secret to 'doing better hydrological science': change the question! Hydrological
944 Processes 23 (9): 1391–1396 DOI: 10.1002/hyp.7242, 2009.

945 Sivapalan, M., Blöschl, G.: Time scale interactions and the coevolution of humans and water. Water
946 Resources Research 51 (9): 6988–7022 DOI: 10.1002/2015WR017896, 2015.

947 Soulsby, C., Birkel, C., Geris, J., Dick, J., Tunaley, C. and Tetzlaff, D.: Stream water age distributions
948 controlled by storage dynamics and non-linear hydrologic connectivity: modelling with high resolution
949 isotope data. Water Resources Research. DOI: 10.1002/2015WR017888, 2015.

950 Soulsby, C., Bradford, J., Dick, J., McNamara, J.P., Geris, J., Lessels, J., Blumstock, M., Tetzlaff, D.: Using
951 geophysical surveys to test tracer-based storage estimates in headwater catchments. Hydrological
952 Processes 30 (23): 4434–4445 DOI: 10.1002/hyp.10889, 2016.

953 Sklash, M.G., Farvolden, R.N.: The role of groundwater in storm runoff. Journal of Hydrology 43 (1): 45–
954 65 DOI: http://dx.doi.org/10.1016/0022-1694(79)90164-1, 1979.

955 Tetzlaff, D., Birkel, C., Dick, J., and C. Soulsby: Storage dynamics in hydropedological units control hillslope
956 connectivity, runoff generation and the evolution of catchment transit time distributions. Water
957 Resources Research, DOI: 10.1002/2013WR014147, 2014.

958 Tian, F. Q. , Hu, H. P. , & Lei, Z. D.: Thermodynamic watershed hydrological model: constitutive relationship.
959 Science in China Series E: Technological Sciences, 51(9), 1353-1369, 2008. Troch, P. A., Carrillo, G.,
960 Sivapalan, M., Wagener, T., Sawicz, K.: Climate-vegetation-soil interactions and long-term hydrologic
961 partitioning: signatures of catchment co-evolution. Hydrology and Earth System Sciences 17 (6): 2209–
962 2217 DOI: 10.5194/hess-17-2209-2013, 2013.

963 Tromp-van Meerveld, H. J. & McDonnell, J. J.: Threshold relations in subsurface stormflow: 1. A 147-storm
964 analysis of the Panola hillslope. Water Resources Research 42. DOI: 10.1029/2004WR003778, 2006.

965 Van Beek, L.P.H. and M.F.P. Bierkens, The Global Hydrological Model PCR-GLOBWB: Conceptualization,
966 Parameterization and Verification, Report Department of Physical Geography, Utrecht University, Utrecht,
967 The Netherlands, http://vanbeek.geo.uu.nl/suppinfo/vanbeekbierkens2009.pdf, 2008.

968 Vrugt, J. A.: Effective and efficient algorithm for multiobjective optimization of hydrologic models. Water
969 Resources Research 39 (8): 1–19 DOI: 10.1029/2002WR001746, 2003.

970 Wang, D., Tang, Y.: A one‐parameter Budyko model for water balance captures emergent behavior in
971 darwinian hydrologic models. Geophysical Research Letters 41 (13): 4569–4577, 2014.

972 Wang, D.: A new probability density function for spatial distribution of soil water storage capacity leads
973 to SCS curve number method, Hydrol. Earth Syst. Sci. Discuss., https://doi.org/10.5194/hess-2018-32, in
974 review, 2018.

975 Wang-Erlandsson, L., Bastiaanssen, W.G.M., Gao, H., Jägermeyr, J., Senay, G.B., van Dijk, A.I.J.M.,
976 Guerschman, J.P., Keys, P.W., Gordon, L.J., Savenije, H.H.G.: Global root zone storage capacity from
977 satellite-based evaporation. Hydrol. Earth Syst. Sci. 20 (4): 1459–1481 DOI: 10.5194/hess-20-1459-2016,
978 2016.

979 Weiler, M., McDonnell, J. J.: Conceptualizing lateral preferential flow and flow networks and simulating
980 the effects on gauged and ungauged hillslopes. Water Resour. Res. 43, W03403, 2007.

981 Wolock, D. M.: STATSGO Soil Characteristics for the Conterminous United States. US Geological Survey,
982 Washington, DC., 1997.

983 Ye, A., Duan, Q., Yuan, X., Wood, E.F., Schaake, J.: Hydrologic post-processing of MOPEX streamflow

984 simulations. Journal of Hydrology 508: 147–156 DOI: 10.1016/j.jhydrol.2013.10.055, 2014.

985 Yu, Z., Lu, Q., Zhu, J., Yang, C., Ju, Q., Yang, T., Chen, X., and Sudicky, E. A.: Spatial and temporal scale effect

986 in simulating hydrologic processes in a watershed. Journal of Hydrologic Engineering, 19(1), 99-107, 2014.

987 Zehe, E., Fluehler, H.: Preferential transport of Isoproturon at a plot scale and a field scale tile-drained site.

988 J. Hydrol. 247, 100–115, 2001.

989 Zehe, E., Ehret, U., Blume, T., Kleidon, A., Scherer, U., Westhoff, M.: A thermodynamic approach to link

990 self-organization, preferential flow and rainfall-runoff behaviour. Hydrol. Earth Syst. Sci. 17 (11): 4297–

991 4322 DOI: 10.5194/hess-17-4297-2013, 2013.

992 Zhao, R-J., Zuang, Y., Fang, L., Liu, X., Zhang, Q.: The Xinanjiang model. Hydrological forecasting —

993 Prévisions hydrologiques (129): 351–356, 1980.

994

995

996 Table 1. The parameters of the models, and their prior ranges for calibration. ([*]S_{uMax} is a parameter in HBV,

997 TOPMODEL and the HSC model, but HSC-MCT model does not have S_{uMax} as a free parameter; [**] β is a parameter in

998 HBV model, but not in TOPMODEL, HSC and HSC-MCT models)

Parameter	Explanation	Prior range for calibration
S_{iMax} (mm)	Maximum interception capacity	2
S_{uMax} (mm) [*]	The root zone storage capacity	(10, 1000)
β (-) [**]	The shape of the storage capacity curve	(0.01, 5)
C_e (-)	Soil moisture threshold for reduction of evaporation	(0.1, 1)
D (-)	Splitter to fast and slow response reservoirs	(0, 1)
T_{lagF} (d)	Lag time from rainfall to peak flow	(0, 10)
K_f (d)	The fast recession coefficient	(1, 20)
K_s (d)	The slow recession coefficient	(20, 400)

999

1000

1001 Table 2. The water balance and constitutive equations used in models. (Function (15)* is used in the HBV model, but

1002 not used in the TOPMODEL, HSC and HSC-MCT models)

reservoirs	Water balance equations	Constitutive equations
Interception reservoir	$\dfrac{\mathrm{d}\,S_i}{\mathrm{d}\,t} = P - E_i - P_e$ (8)	$E_i = \begin{cases} E_p; S_i > 0 \\ 0; S_i = 0 \end{cases}$ (9) $P_e = \begin{cases} 0; & S_i < S_{iMax} \\ P; & S_i = S_{iMax} \end{cases}$ (10)
Unsaturated reservoir	$\dfrac{\mathrm{d}\,S_u}{\mathrm{d}\,t} = P_e - E_a - R_u$ (11)	$\dfrac{R_u}{P_e} = \left(\dfrac{S_u}{S_{uMax}}\right)^{\beta}$ (12)* $\dfrac{E_a}{E_p - E_i} = \dfrac{S_u}{C_e S_{uMax}}$ (13)
Splitter and Lag function		$R_f = R_u D$ (17); $R_s = R_u(1-D)$ (14) $R_{fl}(t) = \sum_{i=1}^{T_{lagf}} c_f(i) \cdot R_f(t-i+1)$ (15) $c_f(i) = i / \sum_{u=1}^{T_{lagf}} u$ (16)
Fast reservoir	$\dfrac{\mathrm{d}\,S_f}{\mathrm{d}\,t} = R_f - Q_f$ (17)	$Q_f = S_f / K_f$ (18)
Slow reservoir	$\dfrac{\mathrm{d}\,S_s}{\mathrm{d}\,t} = R_s - Q_s$ (19)	$Q_s = S_s / K_s$ (20)

1003

1004 Table 3. Data source of the MOPEX catchments.

Data	Unit	Resources	Website	Reference
Daily precipitation	mm/d	MOPEX	http://www.nws.noaa.gov/oh d/mopex/mo_datasets.htm	(Duan et al., 2006)
Daily maximum temperature	ºC	MOPEX	Same as above	Same as above

Daily minimum temperature	°C	MOPEX	Same as above	Same as above
Daily runoff	mm/d	MOPEX	Same as above	Same as above
Aridity index	-	MOPEX	Same as above	Same as above
DEM	m	USGS	http://earthexplorer.usgs.gov/	-
Slope	degree	USGS	Same as above	-
K factor of soil	-	USGS	http://water.usgs.gov/GIS/metadata/usgswrd/XML/muid.xml	(Wolock, 1997; Gao et al., 2018)
Percentage of forest cover	%	NLCD	http://www.mrlc.gov/	(Homer et al., 2015; Gao et al., 2018)
Stream density	Km/km²	Horizon Systems Corporation	http://www.horizon-systems.com/nhdplus/	-
Depth to bedrock	cm	STATSGO	http://www.soilinfo.psu.edu/index.cgi?soil_data&conus&data_cov&dtb	(Schwarz et al., 1995; Gao et al., 2018)

1005

1006

1007   Table 4. Impacts of MOPEX catchment characteristics on model performance (HSC, HBV, and TOPMODEL)

Catchment characteristics	HSC > HBV	HSC ≈ HBV	HSC < HBV	HSC > TOPMODEL	HSC ≈ TOPMODEL	HSC < TOPMODEL
Averaged HAND (m)	37	71	-	27	69	193
Averaged slope (degree)	4.0	5.7	-	3.6	5.6	13.5
Averaged elevation (m)	454	395	-	469	393	740
Averaged K-factor (-)	0.28	0.29	-	0.29	0.29	0.25
Forest proportion (%)	22	43	-	14	43	68
Aridity index (-)	1.1	0.9	-	1.3	0.9	0.8
Stream density (-)	0.72	0.81	-	0.77	0.80	0.83

	Averaged depth to rock (cm)	192	219	-	210	215	333

1008
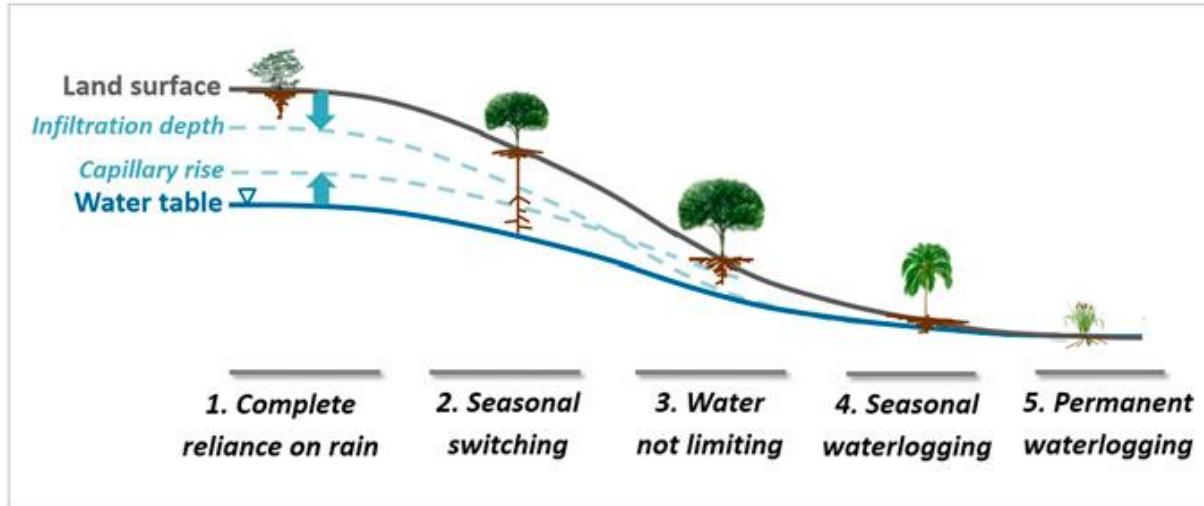
1009

1010 Figure 1. The variation of plant rooting depths along a hillslope profile, showing the impact of HAND

1011 (Height Above the Nearest Drainage) on rooting depth. (Taken from Fan et al., 2017 by permission of PNAS)
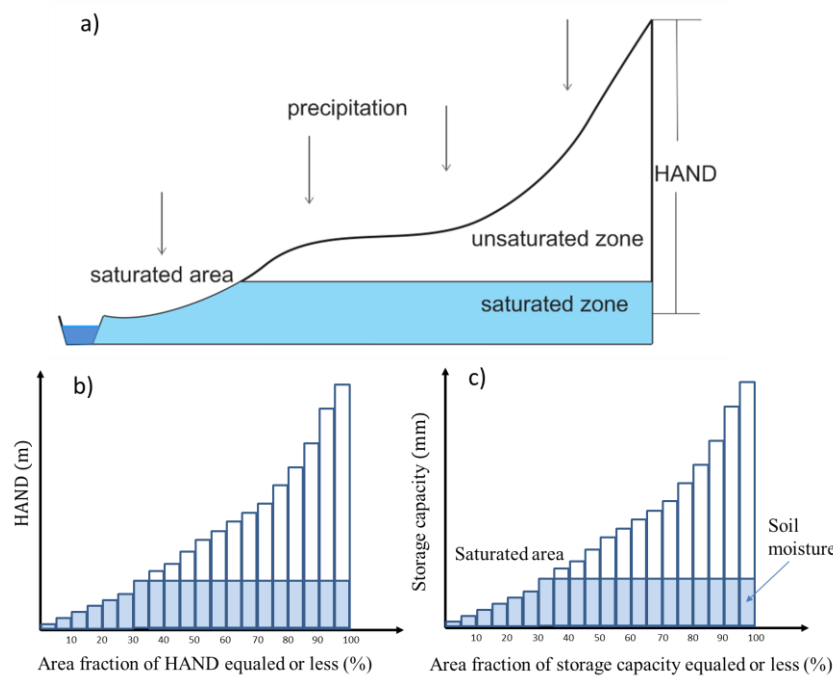
1012

1013 Figure 2. The perceptual model of the HAND-based Storage Capacity curve (HSC) model. a) shows the representative

1014 hillslope profile in nature, and the saturated area, unsaturated zone and saturated zone; b) shows the relationship

1015   between HAND bands and their corresponded area fraction; c) shows the relationship between storage capacity-

1016   area fraction-soil moisture-saturated area, based on the assumption that storage capacity linearly increases with

1017   HAND values.

1018

1019
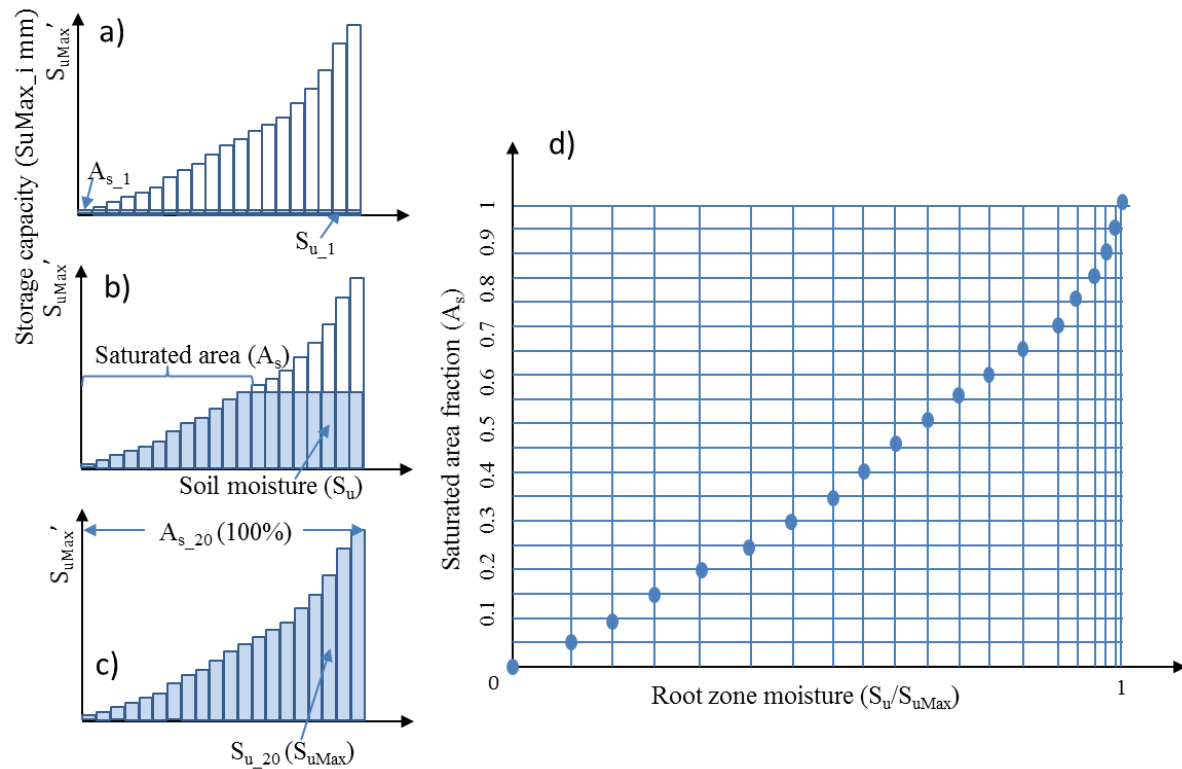
1020

1021   Figure 3. The conceptual model of the HSC model. a), b) and c) illustrate the relationship between soil moisture (S_u)

1022   and saturated area (A_s) in different soil moisture conditions. In d), 20 different S_u-A_s conditions are plotted, which

1023   allow us to estimate A_s from S_u.

1024
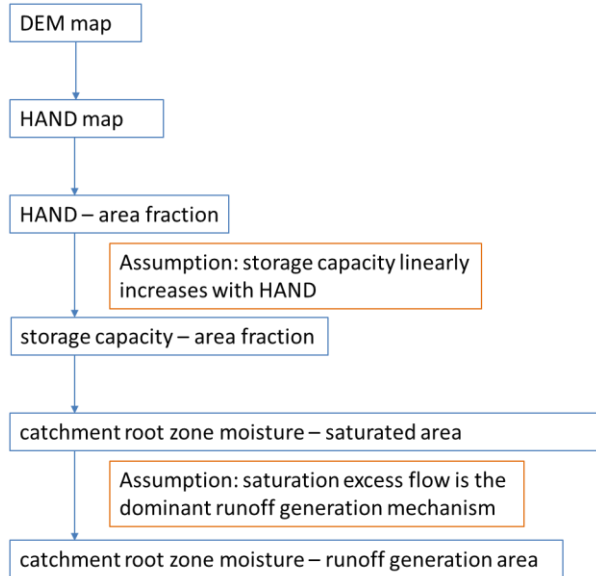
1025

1026   Figure 4. The procedures estimating runoff generation by the HSC model and its two hypotheses.

1027
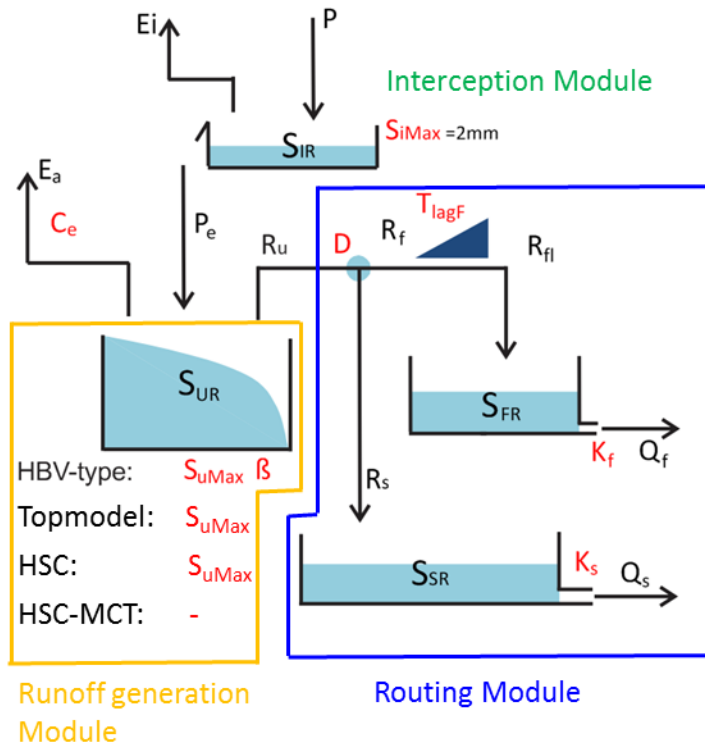
1028

1029   Figure 5. Model structure and free parameters, involving four runoff generation models (HBV-type, TOPMODEL, HSC,

1030   and HSC -MCT). HBV-type has S_{uMax} and beta two free parameters; TOPMODEL and HSC models have S_{uMax} as one

1031   free parameter; and HSC-MCT model does not have free parameter. In order to simplify calibration process and

1032   make fair comparison, the interception storage capacity (S_{iMax}) was fixed as 2mm.

1033

1034
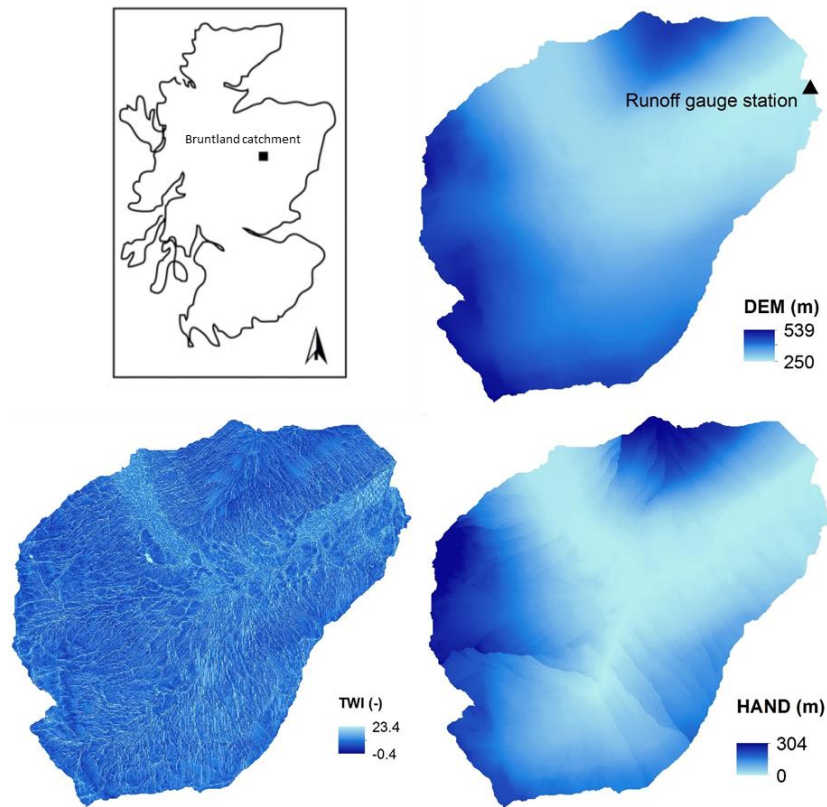
1035

1036   Figure 6. (a) Study site location of the Bruntland Burn catchment within Scotland; (b) digital elevation model (DEM)

1037   of the Bruntland Burn catchment; (c) the topographic wetness index map of the Bruntland Burn catchment; (d) the

1038   height above the nearest drainage (HAND) map of the Bruntland Burn catchment.

1039

1040
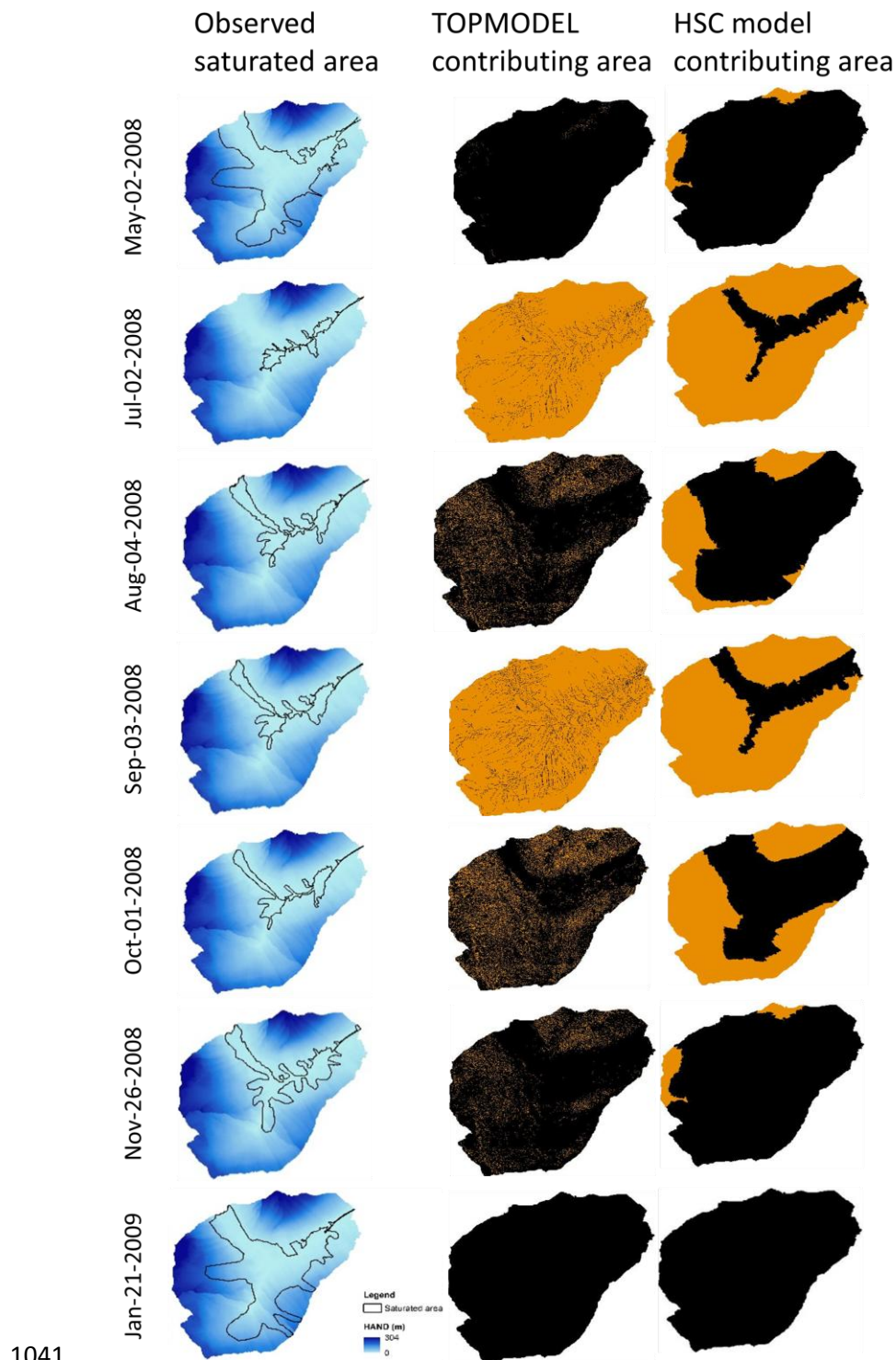
1041

1042   Figure 7. The measured saturated areas and the simulated contributing areas (black) by TOPMODEL and HSC models.

1043

1044
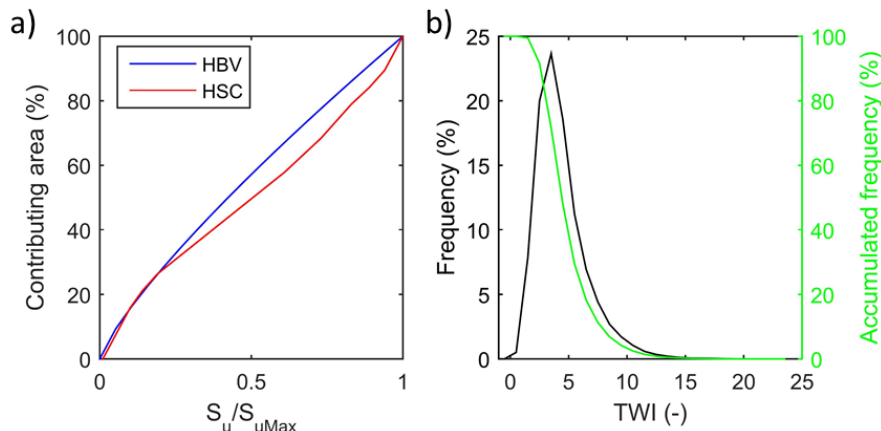
1045

1046   Figure 8. The curves of the beta function of HBV model, and the S_u-A_s curve generated by HSC model (the left figure).

1047   The frequency and accumulated frequency of the TWI in the Bruntland Burn catchment (the right figure).

1048
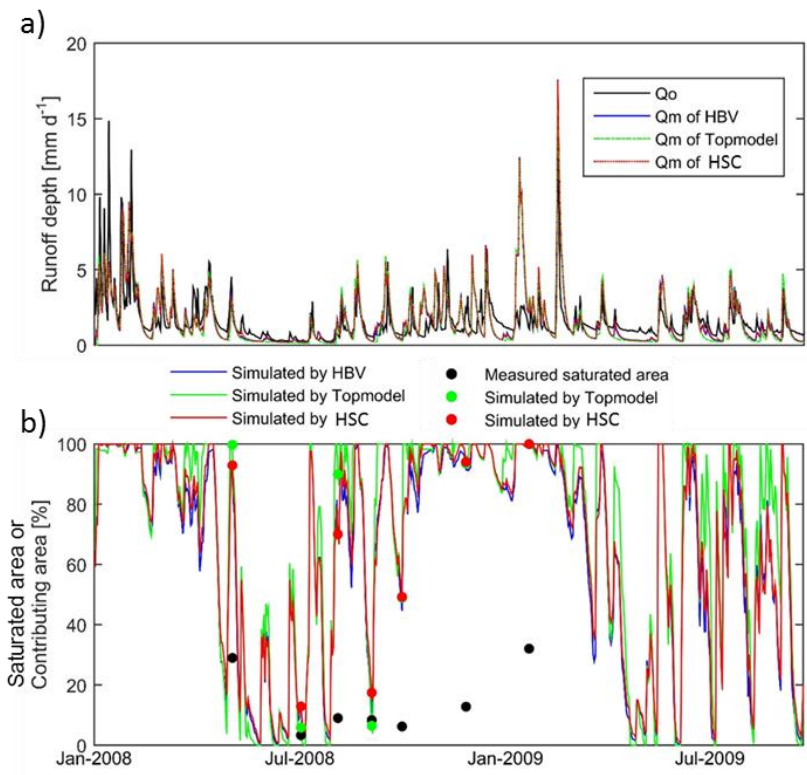
1049

1050   Figure 9. a) The observed hydrograph (Qo, black line) of the Bruntland Burn catchment in 2008. And the simulated

1051   hydrographs (Qm) by HBV model (blue line), TOPMODEL (green dash line), HSC model (red dash line); b) the

1052   comparison of the observed saturated area of 7 days (black dots) and simulated relative soil moistures, i.e. HBV (blue

1053   line), TOPMODEL (green line and dots), HSC (red line and dots).

1054

1055
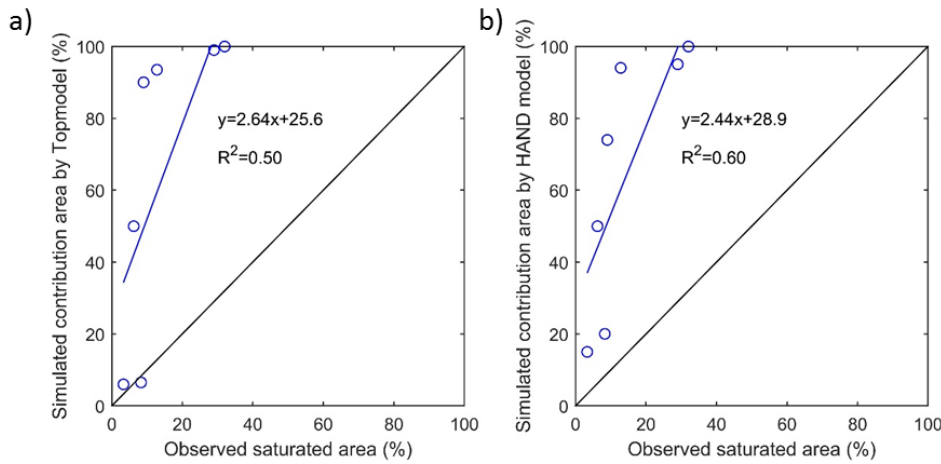
1056

1057   Figure 10. The comparison of the observed saturated area and simulated contributing areas by TOPMODEL and HSC

1058   models.

1059

1060

1061

Figure 11. The Height Above the Nearest Drainage (HAND) map of the CONUS.
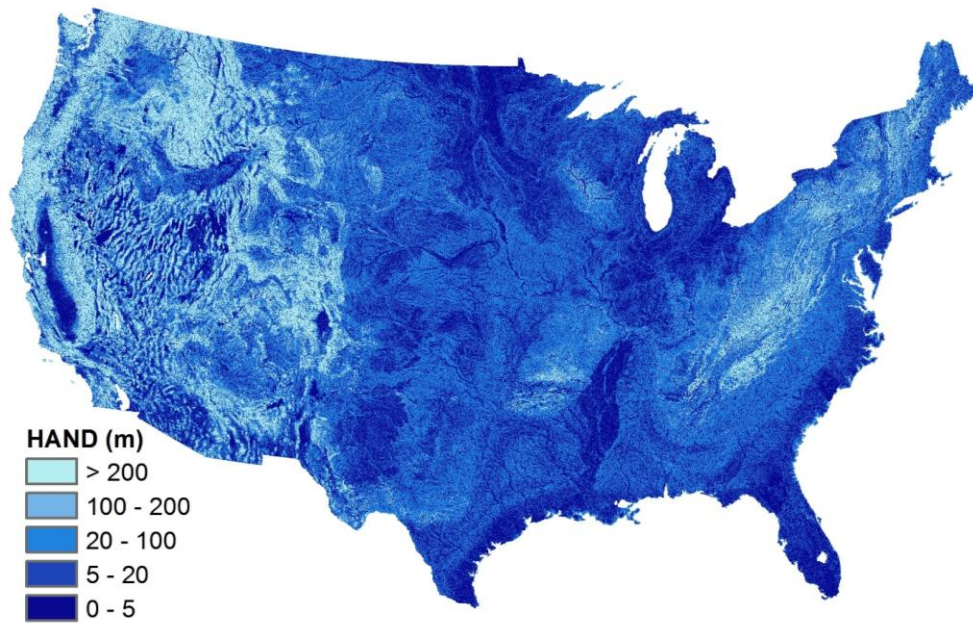
1062

1063   Figure 11. The Height Above the Nearest Drainage (HAND) map of the CONUS.
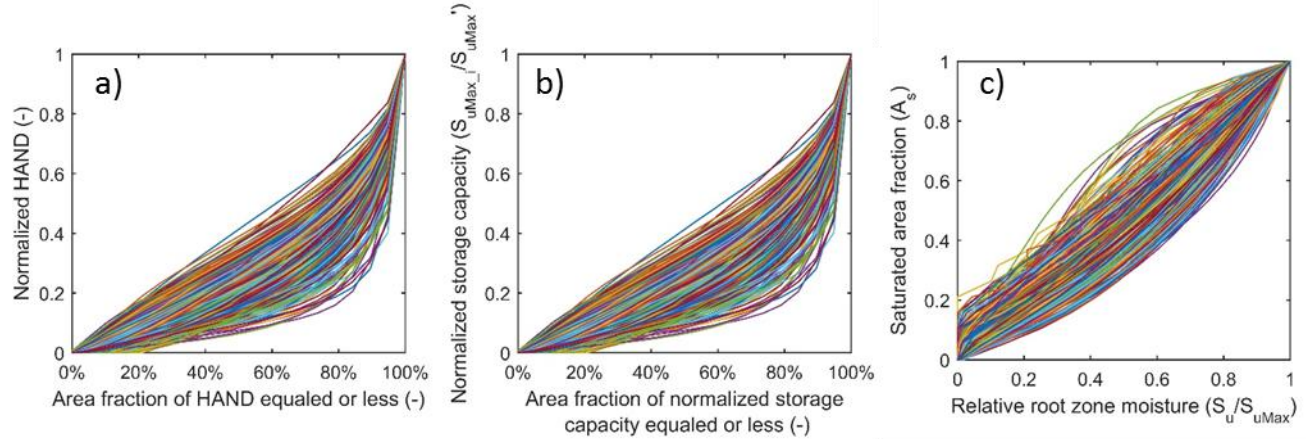
1066

Figure 12. a) The profiles of the normalized HAND of the 323 MOPEX catchments; b) the relations between area
fraction and the normalized storage capacity profile of the 323 MOPEX catchments; c) the S_u-A_s curves of the HSC
model which can be applied to estimate runoff generation from relative soil moisture for the 323 MOPEX catchment.

1070
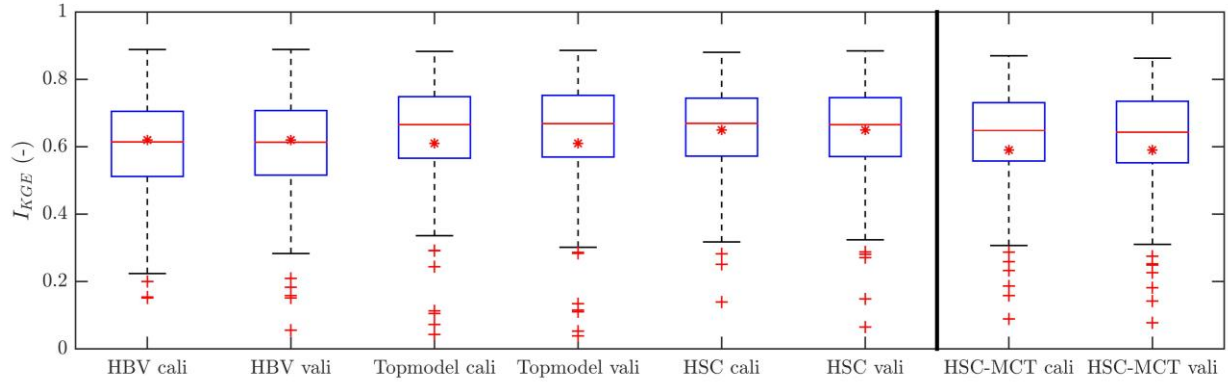
1071

Figure 13. The comparison between the HBV, the TOPMODEL, the HSC, and the HSC-MCT models

1073
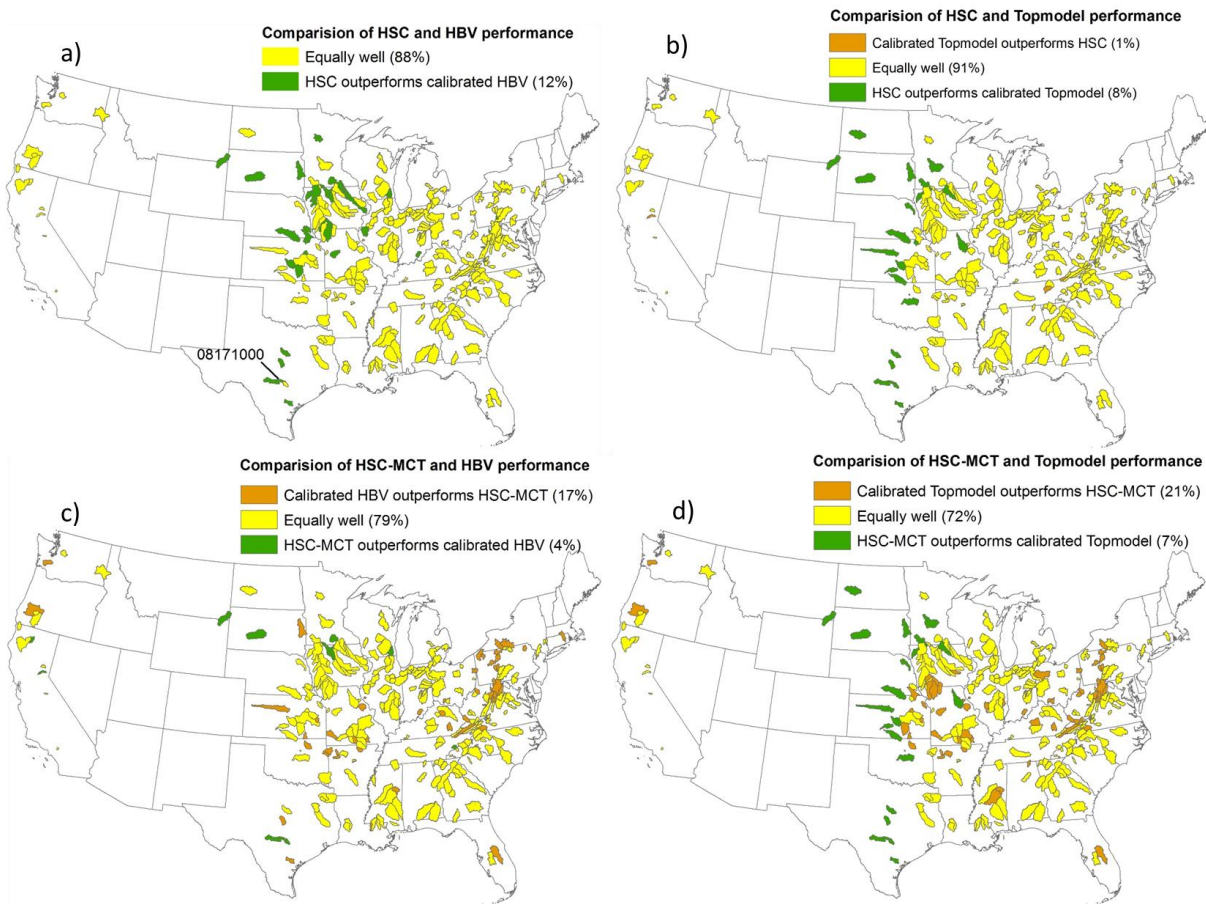
1074

1075 Figure 14. Performance comparison of the HSC and HSC-MCT models compared to two benchmarks models: HBV

1076 and TOPMODEL, for the 323 MOPEX catchments.